the plant journal

SEB SOCIETY FOR EXPERIMENTAL BIOLOGY

The Plant Journal (2025) **121,** e70067 doi: 10.1111/tpj.70067

Excessive leaf oil modulates the plant abiotic stress response via reduced stomatal aperture in tobacco (*Nicotiana tabacum*)

Katherine M. Murphy[1], Brandon S. Johnson[2], Courtney Harmon[1], Jorge Gutierrez[1], Hudanyun Sheng[1], Samuel Kenney[1], Katia Gutierrez-Ortega[1], Janithri Wickramanayake[1], Annika Fischer[1], Autumn Brown[1], Kirk J. Czymmek[1], Philip D. Bates[2], Doug K. Allen[1,3,*] and Malia A. Gehan[1,*]

[1]*Donald Danforth Plant Science Center, 975 N. Warson Rd, St. Louis, Missouri 63132, USA,*
[2]*Washington State University, Pullman, Washington 99164, USA, and*
[3]*USDA ARS, St. Louis, Missouri 63132, USA*

Received 11 June 2024; revised 13 February 2025; accepted 17 February 2025.
*For correspondence (e-mail doug.allen@ars.usda.gov and mgehan@danforthcenter.org).

SUMMARY

High lipid producing (HLP) tobacco (*Nicotiana tabacum*) is a potential biofuel crop that produces an excess of 30% dry weight as lipid bodies in the form of triacylglycerol. While using HLP tobacco as a sustainable fuel source is promising, it has not yet been tested for its tolerance to warmer environments that are expected in the near future as a result of climate change. We found that HLP tobacco had reduced stomatal conductance, which results in increased leaf temperatures up to 1.5°C higher under control and high temperature (38°C day/28°C night) conditions, reduced transpiration, and reduced CO_2 assimilation. We hypothesize this reduction in stomatal conductance is due to the presence of excessive, large lipid droplets in HLP guard cells imaged using confocal microscopy. High temperatures also significantly reduced total fatty acid levels by 55% in HLP plants; thus, additional engineering may be needed to maintain high titers of leaf oil under future climate conditions. High-throughput image analysis techniques using open-source image analysis platform PlantCV for thermal image analysis (plant temperature), stomata microscopy image analysis (stomatal conductance), and fluorescence image analysis (photosynthetic efficiency) were developed and applied in this study. A corresponding set of PlantCV tutorials are provided to enable similar studies focused on phenotyping future crops under adverse conditions.

Keywords: abiotic stress, high temperature, heat stress, *Nicotiana tabacum*, biofuel, triacylglycerol, phenotyping, stomata, photosynthesis.

INTRODUCTION

Global temperatures are expected to increase by 0.3–4.8°C by the year 2100 (IPCC, 2014), threatening production of crops and livestock as a result of climate change. The production of oil in plants for food and fuel holds significant potential to supplant energy generation from fossil-fuel sources, directly addressing a cause of climate change for a more sustainable future (Carlsson et al., 2011; El-Araby, 2024). However, while oil crops provide an opportunity to reduce future net carbon emissions, they must be able to thrive in the anticipated rising global temperatures that adversely affect plant growth, size, reproduction, and potentially oil production (Chaudhry & Sidhu, 2022; Jagadish et al., 2021). This requires a better understanding of plant processes in high temperatures, including how current and future crops respond to temperature stress conditions.

In an effort to produce high levels of oil in non-seed tissues as a fuel source, a recent study generated a high lipid producing (HLP) tobacco plant (*Nicotiana tabacum*) that produced up to 30% of the plant dry weight as oil, primarily as triacylglycerol (TAG) (Vanhercke et al., 2017). This is a substantial increase compared with the ~0.1% TAG content by dry weight of wild-type (WT) tobacco plants (Vanhercke et al., 2017). This oil increase primarily consisted of TAG in oil bodies in the leaf mesophyll cytoplasm (Vanhercke et al., 2017). To accomplish this goal, HLP contained the addition of four genes: transcription factors WRI1 (WRINKLED1) and LEC2 (LEAFY COTYLEDON2), biosynthetic enzyme DGAT1 (Acyl-CoA:diacylglycerol

acyltransferase 1), and oil-body stabilization protein OLEOSIN (Vanhercke et al., 2014, 2017). In addition to increased oil content, HLP plants exhibited a reduction in leaf starch content, reduced carbon assimilation, and a slight reduction in plant size (Chu et al., 2022; Vanhercke et al., 2017). The tolerance of HLP to abiotic stress has not yet been investigated. Therefore, understanding how HLP responds to high temperature conditions will be critical to ensuring high levels of oil production amid rising global temperatures.

High temperature stress impacts plant survival, size, and yield, threatening oil production in biofuel crops such as HLP. While extreme heat (20°C higher than average growth conditions) may result in rapid cell death, even moderate increases in air temperatures (5–12°C higher than average growth conditions) reduce plant growth rates, resulting in a smaller plant sizes (Allakhverdiev et al., 2008; Bita & Gerats, 2013; Chaudhry & Sidhu, 2022; Hasanuzzaman et al., 2013). Tolerance and susceptibility are two ends of a spectrum of abiotic stress responses; here we define "tolerant" as the genotype with a selected phenotype most similar to control treatment and "susceptible" as the most different from control. Plants can mitigate the effects of high temperature through acclimation (the capacity to increase tolerance to an environment within an organism's lifetime), avoidance (changing plant structure or activity to survive under stress), or escape (completion of life cycle), with mechanisms described below (Zhu et al., 2021). The ability of plants to acclimate and avoid high temperature stress makes them more tolerant to these stressors. In the case of HLP, total oil yield is related to both plant size and amount of oil per gram of leaf tissue, therefore maintaining both phenotypes is critical to yield under stress conditions.

High temperature stress reduces thus plant size by decreasing photosynthetic efficiency and reducing carbon assimilation (Allakhverdiev et al., 2008; Bita & Gerats, 2013; Chaudhry & Sidhu, 2022; Hasanuzzaman et al., 2013). Underlying these changes in photosynthesis are changes in the stability of membranes, proteins, and other cellular components, as well as changes in photosynthetic enzyme activity and mesophyll conductance, that are directly affected by increased temperatures (Allakhverdiev et al., 2008; Bernacchi et al., 2001, 2002, 2003; Bita & Gerats, 2013; Hasanuzzaman et al., 2013; Mathur et al., 2014). A major factor underlying temperature stress outcomes are the lipid-based cell and chloroplast membranes, which impact downstream photosynthesis, plant size, and survival. At a single temperature, membrane fluidity is determined by the composition and degree of unsaturation of lipids – greater unsaturation results in lower viscosity (Allakhverdiev et al., 2008; He & Ding, 2020) – and temperature at least partially determines membrane composition during plant growth (Barber et al., 1984). Thus, as plants acclimate and/or adapt to high temperatures, membrane compositions adjust to tolerate changes in temperature (Mathur et al., 2014). Chloroplast membranes, in particular, are acutely sensitive to high temperatures, and modifications to these lipid membranes are critical to stress tolerance (Bita & Gerats, 2013; Hu et al., 2020). Under high temperatures, thylakoid membranes become unstable, grana swell, and grana stacking becomes compromised (Bita & Gerats, 2013; Mathur et al., 2014). With increasing disorder, photosystem proteins are physically dislodged from membranes (Bita & Gerats, 2013; Mathur et al., 2014), decreasing photosynthesis and providing opportunities for reactive oxygen species (ROS) generation. As ROS increases, membrane lipids are subject to peroxidation, and thus further damage as a result of high temperature stress (dos Santos et al., 2022).

In addition to their involvement in membranes, lipids in the form of droplets or oil bodies are important to temperature stress acclimation. In plants, TAG lipid droplets accumulate in vegetative tissues in response to abiotic stress and serve as a potential location to sequester intermediates of lipid turnover that would otherwise become toxic if concentrations increased throughout the cell (Lu et al., 2020). In addition, the lipid droplets provide binding sites for lipid droplet-associated proteins, specifically those necessary for membrane-remodeling for fluidity adjustments (Lu et al., 2020). For example, Murakami et al. (2000) demonstrated that gene silencing in the trienoic polyunsaturated fatty acid biosynthesis pathway in *N. tabacum* increased high temperature stress acclimation. However, an increase in lipid oil bodies is not always beneficial. Yurchenko et al. (2018) found that when vegetative tissue was engineered to increase leaf oil content in *Arabidopsis thaliana*, plants were more susceptible to long-term heat stress, resulting in more plant death compared with control.

While high temperatures impact lipids and thus downstream photosynthesis, there are mechanisms by which a plant can mitigate the effects of increased temperatures. Producing osmoprotectants and specialized metabolites and altering transcription are examples of acclimation mechanisms (Mathur et al., 2014). Stomata, the pores on leaves that facilitate gas exchange, act as both an entry point for carbon dioxide for photosynthesis, as well as an exit for water evaporating from the leaf. Open stomata promote transpirational cooling, or the cooling of leaves via the evaporation of water, which reduces the plant leaf temperature (Sadok et al., 2021). Changing leaf orientation and transpirational cooling are examples of avoidance mechanisms in response to high temperatures (Mathur et al., 2014). Stomata respond to changing conditions, including air temperature, water status, and light intensity, via the action of guard cells around the stomatal pore. These adjustments influence both the transpirational

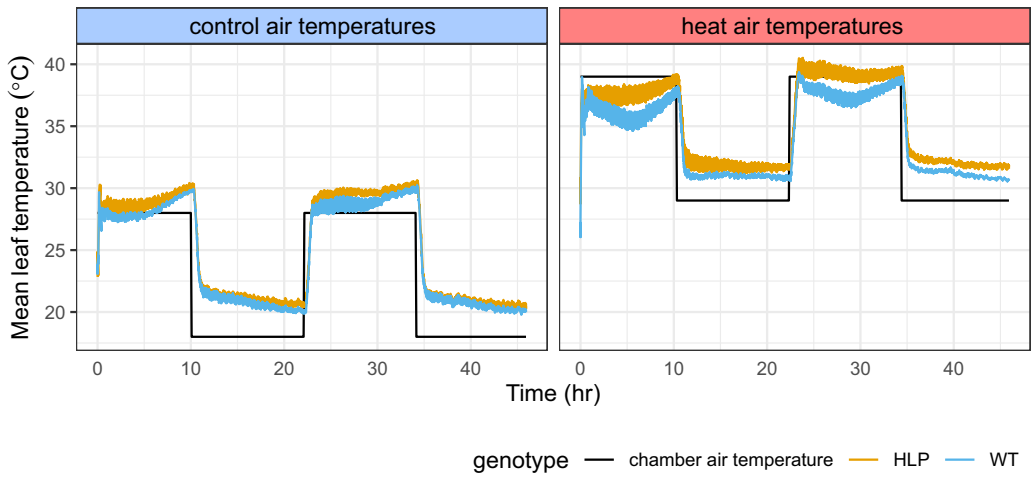

Figure 1. High lipid producing (HLP) tobacco had higher leaf temperatures than WT.
Mean leaf temperature was measured using an infrared thermography camera every 15 min, and averaged per plant and per genotype under control and heat stress conditions. Lights were kept on for the duration of this measurement to maintain camera focus. $n = 4$ plants per genotype and treatment.

cooling and carbon assimilation (open stomata) and water conservation (closed stomata) (Faralli et al., 2021; Farquhar & Sharkey, 1982; Rivero et al., 2022). While there is a trade-off between water loss via transpiration and carbon assimilation, there is not a rebalancing of leaf cooling (Ranawana et al., 2023). Stomatal conductance is also intimately tied to lipid metabolism because guard-cell TAG is necessary for stomatal opening (McLachlan et al., 2016); therefore, attempts to increase lipid levels in plant tissues must account for potential off-target effects such as increased or decreased stomatal size, number, distribution, responsiveness, and speeds of opening and closing. The details of HLP stomata compared with WT, including aperture size, number of stomata, and a possible difference in guard cell oil have yet to be investigated, and thus, the possible impacts on leaf temperature regulation are unknown.

Given the wide importance of lipids to membranes and oil bodies, and the conflicting results of prior research that suggests oil bodies could be a benefit or detriment under high temperature stress, predicting HLP plant response under high temperature is complex. We hypothesized that a reduction in photosynthesis under high temperatures would reduce oil yield in HLP because of the carbon-rich nature of lipids. One hypothesis is that increased oil bodies may provide a source of lipids for membrane modification to appropriate fluidity, as well as a sequestration site for toxic lipid intermediates, providing greater tolerance measured by plant size and photosynthetic efficiency than WT under increased temperatures. On the other hand, the high levels of engineered lipid flux to oil bodies coated in oleosin may instead reduce available lipids for membrane modifications and increase high temperature susceptibility, decreasing plant size and photosynthetic efficiency.

Future biofuel crops provide an opportunity to reduce net carbon emissions, but it is important to evaluate them in future climate scenarios. In this study, we examined the response of HLP tobacco to high temperature. Combining multiple techniques in plant thermal imaging, microscopy, fluorescence imaging, and whole-plant transpiration, we describe the stress response of HLP relative to WT, as well as the altered mechanisms of stress avoidance in HLP. Assessment of leaf oil content, in addition to changes at the whole-plant level, are critical to understanding the oil yields of this crop and how it will fare in future climates.

RESULTS AND DISCUSSION

HLP tobacco had increased leaf temperatures, especially under high temperature conditions

Plant transpiration is a major determinate of leaf temperature. Given that the biochemical changes due to heat stress are dependent on leaf rather than air temperature, measurements of leaf surfaces can be an indicator of heat stress tolerance (Jagadish et al., 2021). Therefore, we used thermal imaging with a forward-looking infrared (FLIR) camera to measure leaf surface temperatures under control and high temperature conditions for 48 h, with constant light and humidity. Image analysis was performed using new thermal image analysis functions in PlantCV, with an interactive tutorial accompanying this study (see "Materials and Methods" section) (Fahlgren et al., 2015; Gehan et al., 2017).

Genotype was a significant factor in mean leaf temperature ($P < 0.0001$, Figure 1). This difference was largest under high temperature conditions, where HLP plants were ~1.5°C warmer than WT in both day and "night" (when lights were kept on for imaging but temperature changed

to night conditions) ($P < 0.001$, Figure 1). Under control conditions, HLP had an average daytime leaf temperature of 29.75°C with a variance of 0.02°C on Day 2, while WT had an average 29.05°C with a variance of 0.00004°C. In high temperature conditions, HLP had an average daytime leaf temperature of 39.29°C with a variance of 0.001°C on Day 2, while WT had an average 37.72°C with a variance of 0.005°C. WT plants also showed greater fluctuation in temperatures over the course of the day, measured by a significantly higher variance around the mean daytime leaf temperature ($P < 0.001$ between genotypes for both treatments, Figure 1). This was especially apparent under high temperature, possibly indicating a greater responsiveness in WT than HLP (Figure 1).

HLP tobacco had reduced stomatal aperture and stomatal conductance

Leaf temperatures are tied to evaporative transpiration, which is largely determined by stomatal conductance (g_{sw}). Stomatal conductance is determined by both the number of stomata per unit leaf area and the size of the stomatal opening (also called aperture) (Lawson & Vialet-Chabrand, 2019). Since HLP plants had differences in leaf temperature compared with WT, we used non-destructive leaf impressions to measure the number and aperture of stomata under control and high temperature conditions. We developed a high-throughput method in PlantCV to analyze stomatal impression microscopy images, which quantifies both the number of stomata, as well as the aperture (defined here as the area of the center of the two guard cells that appears darker in imaging), which substantially increased the throughput of brightfield microscopy image analysis. An interactive tutorial for analyzing stomatal images is available with this study (see "Materials and Methods" section) (Murphy, 2024). The method is generalizable to researchers collecting similar types of stomatal images.

HLP plants had a mean aperture of $145 \pm 4.2\,\mu m$ while WT had a mean aperture of $168 \pm 3.3\,\mu m$ under control conditions. This increased to 230 ± 6.2 and $253 \pm 5.0\,\mu m$, respectively, under high temperature. Therefore, stomatal aperture was significantly smaller in HLP compared with WT plants under both control and after 24 hours of high temperature conditions ($P < 0.05$ in control, $P < 0.01$ in high temperature) (Figure 2A). HLP plants also had significantly fewer stomata than WT under both control ($P < 0.05$) and high temperature ($P < 0.01$) conditions (Figure 2B). While HLP plants had a mean of 24 ± 3 stoma per unit leaf area in control and 39 ± 2 stoma in high temperature, WT had a mean of 35 ± 3 stoma and 54 ± 4 stoma in the control and high temperature conditions, respectively. Both genotypes demonstrated a significant increase in aperture ($P < 0.0001$) and number of stomata ($P < 0.01$) between control and high temperature conditions (Figure 2). Previous research showed that the number of epidermal cells

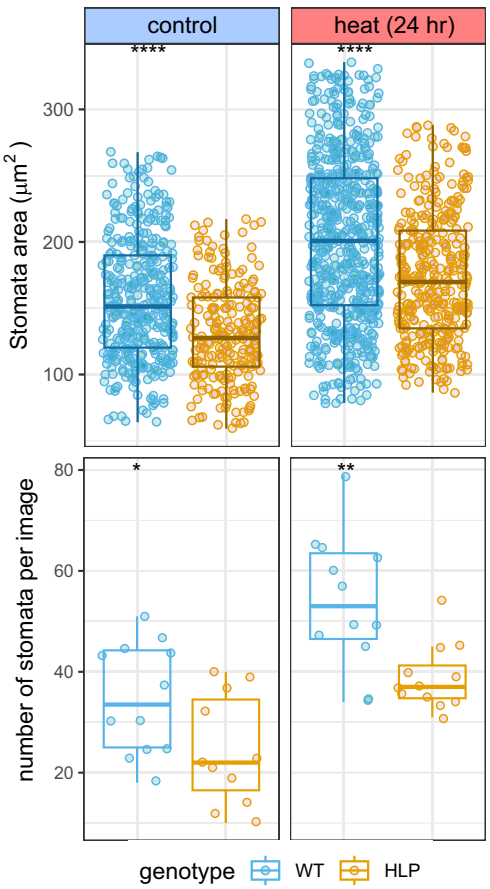

Figure 2. High lipid producing (HLP) tobacco had smaller stomatal aperture and fewer stomata per leaf than WT.
Stomatal aperture and number were measured using image analysis of brightfield microscopy images after 24 h of heat stress. *$P < 0.1$, **$P < 0.01$, ****$P < 0.0001$. $n = 4$ plants per genotype and treatment, three images per plant.

per leaf area (and thus the size of the epidermal cells) was not significantly different between the genotypes, suggesting this change is specific to the stomata, and not a more pervasive change in cell size in HLP (Johnson et al., 2025). Together, the same number of epidermal cells but reduced number of stomata per unit leaf area equated to a reduced stomatal index for HLP.

Following this result, stomatal conductance and its dynamic change over time under control and high temperature conditions were further investigated with a LiCOR Li-6800 portable photosynthesis system (LI-COR, Lincoln, NE, USA). The temperature within the Li-6800 leaf chamber was held for 24 min at control temperature, matching the growth conditions, and the leaf chamber (but not the growth chamber) was subsequently increased and held for 24 min at high temperature conditions under constant light to allow for stabilization of stomatal conductance under each temperature condition. Leaf temperature measured

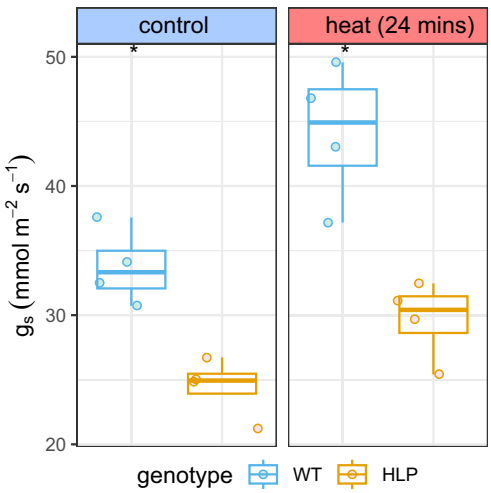

Figure 3. High lipid producing (HLP) had lower stomatal conductance than WT.
Stomatal conductance (g_s) measured using a portable photosynthesis meter. $n = 4$ plants per genotype and treatment. *$P < 0.1$.

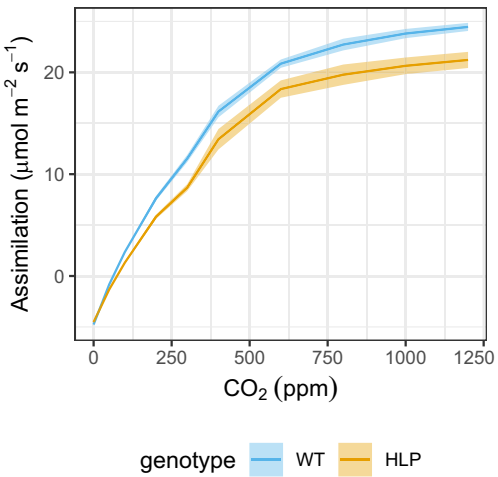

Figure 4. High lipid producing (HLP) had a lower assimilation rate than WT. A/Ci curve under control conditions. Shaded ribbon reflects standard error of the mean. A, assimilation, Ci, internal CO_2. $n = 4$ plants per genotype.

using a thermocouple in the Li-6800 corroborated the thermal imaging data; HLP leaf temperatures were higher than WT under both control and high temperature conditions ($P < 0.05$, Figure S1). HLP had a mean leaf temperature of 28.1 ± 0.04°C under control conditions and 34.7 ± 0.05°C after 24 min of high temperature, while WT had a mean leaf temperature of 27.7 ± 0.09°C under control and 34.1 ± 0.10°C after 24 min of high temperature (Figure S1).

As expected, stomatal conductance significantly increased when conditions changed from control to high temperature for both genotypes (Lawson & Vialet-Chabrand, 2019). HLP conductance increased from a mean of 24.5 ± 1.16 mmol m^{-2} sec^{-1} in control to 29.7 ± 1.53 mmol m^{-2} sec^{-1} after 24 min of high temperature, while WT conductance increased from a mean of 33.7 ± 1.45 to 44.1 ± 2.68 mmol m^{-2} sec^{-1} in the same temperature scenario (Figure 3). Furthermore, stomatal conductance was significantly lower in HLP compared with WT under both control and high temperature conditions ($P < 0.01$, Figure 3), which aligned with stomatal imaging data (Figure 2). While WT stomatal conductance had a 30% increase due to heat compared with control, HLP had only a 21% increase. However, this difference in the percent change in conductance was not significantly different due to genotype ($P = 0.08$, Figure 3). These data suggest HLP is still responsive to changes in temperature, and that the stomatal conductance remains lower than WT in both temperature conditions.

HLP tobacco had reduced carbon assimilation and transpiration

Given the observed changes in stomatal conductance, we hypothesized a corresponding change in carbon assimilation and transpiration as a result. Net carbon assimilation was measured using a LiCOR Li-6800 portable photosynthesis system while adjusting the CO_2 level in the LiCOR leaf chamber. Under control conditions, WT had higher overall carbon assimilation than HLP ($P < 0.0001$ for all CO_2 above 200 ppm, Figure 4). WT had a lower CO_2 compensation point (i.e., the CO_2 concentration at which assimilation crosses 0 to become positive) at 54.1 ± 4.79 ppm compared with HLP at 70.1 ± 5.14 ppm; however, this difference was not statistically significant ($P = 0.06$, Figure 4). WT also reached a higher maximum mean assimilation of 24.5 ± 0.32 µmol m^{-2} sec^{-1}, while HLP had a maximum of 21.2 ± 0.56 µmol m^{-2} sec^{-1} ($P < 0.001$, Figure 4).

At each chamber CO_2 setting (ambient CO_2, also termed Ca), the ratio of intracellular CO_2 (Ci) to Ca (termed Ci/Ca) was calculated to determine the amount of CO_2 internalized to the plant cells as another interpretation of the A/Ci curve. Below 100 ppm CO_2 set point, HLP had a significantly higher Ci/Ca (i.e., more internalized CO_2) than WT ($P < 0.01$, Figure S2). However, at 300 and 400 ppm CO_2, the closest setpoints to ambient levels, WT had a higher Ci/Ca ($P < 0.001$, Figure S2). There was no significant difference when Ca was at levels above ambient at 600 ppm and above ($P > 0.05$, Figure S2). The observed lower assimilation and lower Ci/Ca in HLP may be due to stomatal conductance, a conclusion from previous research on stomatal mutants in rice (*Oryza sativa* L.) (Kusumi et al., 2012).

Changes in stomatal conductance may also result in altered water-use dynamics, given stomata are also the primary method of plant transpiration. To investigate transpiration on the whole-plant level, a Ditech Plantarray system (Plant-Ditech, Yavne, Israel) was used to weigh the plants every 3 min under control and high temperature conditions

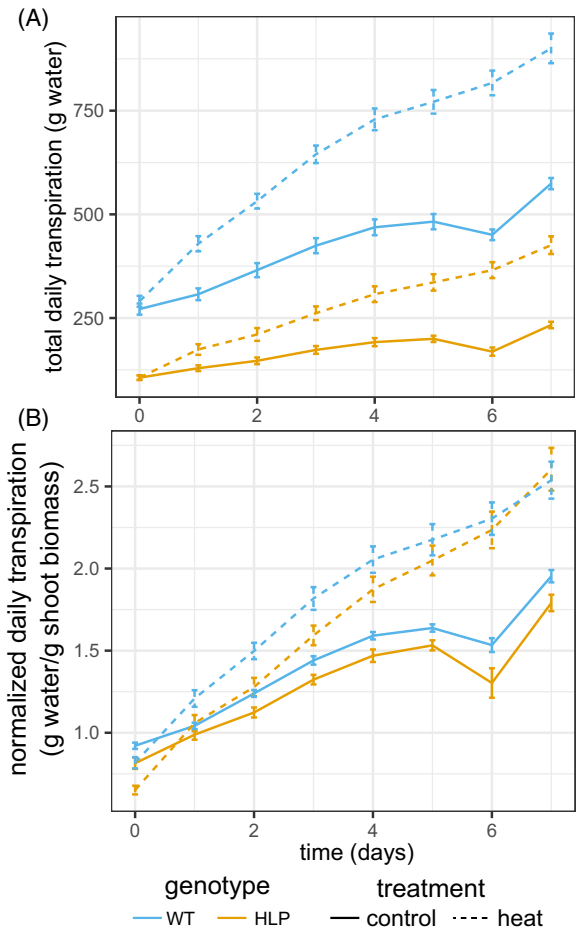

Figure 5. High lipid producing (HLP) had lower transpiration than WT.
(A) Total daily transpiration measured under control (solid line) and heat stress (dotted line) conditions by measuring total pot weight in the morning and the evening on the DiTech Plantarray.
(B) Normalized total daily transpiration, calculated by dividing the total daily transpiration by the wet shoot biomass weighed on Day 7. $n = 4$ plants per genotype and treatment.

for 7 days (Dalal et al., 2020). Both WT and HLP had increased total transpiration in high temperature compared with control at all timepoints after Day 1 ($P < 0.0001$, Figure 5A). While WT had higher total transpiration on Day 1 in high temperature than control ($P < 0.0001$), HLP was not significantly different until Day 2, suggesting HLP was slower to respond to the high temperatures. WT had higher total daily transpiration (amount of water transpired in a day) than HLP under both conditions at all timepoints ($P < 0.0001$, Figure 5A). Because WT plants were larger than HLP plants (Chu et al., 2022; Vanhercke et al., 2017) and larger plants typically transpire more water, the normalized total daily transpiration was calculated as the daily transpiration per g of shoot tissue weighed on the last day of the experiment. WT had greater normalized transpiration than HLP across most of the timecourse ($P < 0.0001$ on Days 2 and 3 in high temperature, and Day 6 in control, Figure 5B).

Together, these data suggest HLP tobacco had increased leaf temperatures, decreased transpiration, and decreased CO_2 assimilation compared with WT because of reduced stomatal conductance (both aperture and number of stomata). These phenotypes were statistically significant in both temperature conditions, and the difference became more extreme under high temperature conditions, and was significant at many timepoints even when transpiration was normalized to plant biomass.

High temperature had modest effects on HLP and WT tobacco biomass

Measuring plant biomass is one important way to assess plant responses to stress and is particularly important when the product of interest is made in leaves, as is the case for HLP. Previous studies on HLP demonstrated a modest reduction in biomass and plant size even under optimal growth conditions (Chu et al., 2022; Vanhercke et al., 2014). We hypothesized this reduction was due to reduced carbon assimilation as a result of reduced stomatal conductance in HLP, and that this reduction in size would also be observed under high temperatures. To assess the impact of high temperature on these traits, we measured plant biomass, leaf area, and leaf number, given that leaf number is a suitable reflection of the developmental stage of the plant. There was no significant difference in the number of leaves due to genotype or treatment ($P > 0.1$), suggesting no change to the developmental stage of the plants. Consistent with previous research, HLP had a smaller leaf area, dry weight, and wet weight than WT under both control and high temperature conditions ($P < 0.0001$, Figure 6). There was also no significant difference in specific leaf area – a ratio of leaf area to dry biomass – between the genotypes within a temperature regime, or due to treatment within a genotype ($P > 0.05$). This suggests that the observed changes in carbon assimilation are not attributed to possible differences in specific leaf area, and are more likely due to stomatal conductance.

After 7 days of high temperature, neither genotype had a reduced leaf area due to treatment ($P > 0.05$, Figure 6A). High temperature significantly increased the wet weight of WT but not HLP ($P < 0.01$ for WT), but had no effect on the dry weight of either genotype ($P > 0.1$, Figure 6B,C). This lack of difference in plant dry weight due to high temperature suggests that, when provided with sufficient water, *N. tabacum* may produce sufficient biomass under future climate conditions, and thus be a good chassis for this example of oil, as well as other economically important bioproducts. The increase in wet weight due to heat stress, therefore, was due to increased water content; when measuring water weight as a percentage of total wet shoot weight, high temperature significantly

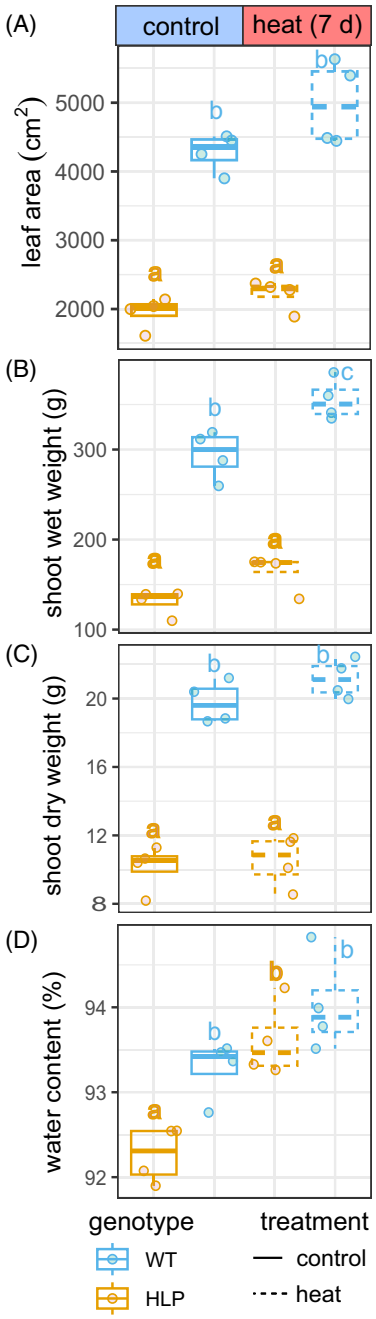

Figure 6. Heat stress increased shoot wet weight in both genotypes.
All plants measured following DiTech Plantarray measurements of transpiration and heat stress treatment (7 days).
(A) Leaf area measured from images of leaves removed from the plant, analyzed using PlantCV. Shoot (leaf and stem) wet weights (B) and dry weights (C).
Percentage water content (D) calculated as (wet weight − dry weight)/(wet weight). Letters represent significantly different groups ($P < 0.05$, ANOVA with LSMEANS *post hoc* test). $n = 4$ plants per genotype and treatment.

increased water content in HLP, but not WT ($P < 0.05$, Figure 6D). This observed increase in water content may be due to reduced transpiration in HLP compared with WT plants. The lack of a significant change in leaf number, leaf area, or dry weight may be due to the duration of stress, intensity of the heat, or the developmental stage of the plant. However, these conditions are both consistent with real-world future temperature expectations (IPCC, 2014), and high temperature treatment did cause significant changes in leaf temperature, carbon assimilation, and transpiration.

High temperature had unique effects on HLP photosynthetic efficiency and stress indices

In addition to possible changes in plant size, measures of photosynthesis and vegetative indices are established indicators of plant health in response to stress conditions (Baker, 2008; Murchie & Lawson, 2013; Sánchez et al., 2015). F_v/F_m is the maximum quantum efficiency of photosystem II photochemistry and is measured on dark-adapted plants; F'_q/F'_m is a light-adapted measurement of photosystem II operating efficiency (Baker, 2008). Non-photochemical quenching (NPQ) uses dark- and light-adapted measurements and represents the heat loss induced by light (Baker, 2008). Higher values of NPQ and lower F'_q/F'_m or F_v/F_m suggest plants are less efficiently converting light energy in the photosynthesis light reactions and are measurements commonly associated with plant health evaluations (Sánchez et al., 2015). Fluorescence plant imaging using a PhenoVation (Wageningen, The Netherlands) CropReporter camera system enabled measurement of F_v/F_m, F'_q/F'_m, NPQ, chlorophyll index, and anthocyanin index from a top-view image of leaf and shoot tissue (Baker, 2008; Murchie & Lawson, 2013; Sánchez et al., 2015). Images were analyzed using PlantCV; see "Materials and Methods" section for a detailed tutorial (Casto et al., 2021).

F_v/F_m was not significantly different due to genotype under control conditions at any time point (Figure 7A). Similarly, F'_q/F'_m was not significantly different due to genotype at Days 1–7 under control conditions ($P > 0.01$); although, there was a small but significant difference between HLP and WT at Day 0 under control conditions ($P < 0.01$, Figure 7B). In contrast, NPQ was statistically greater ($P < 0.01$) in HLP than WT under control conditions at most time points (Days 1, 2, 3, 4, and 6) (Figure 7C). These data suggest that NPQ, but not F_v/F_m or F'_q/F'_m, was higher in HLP than WT under control conditions; in other words, both maximum and quantum efficiency of photosystem II were unaffected by excessive leaf oil, but that the release of excess light energy as heat (NPQ) was higher, and may contribute to reduced photosynthesis in HLP even in ideal conditions.

Under abiotic stress conditions, F_v/F_m and F'_q/F'_m are known to decrease while NPQ is known to increase (Sánchez et al., 2015). The magnitude of these responses is reflective of the stress level of the plant (Sánchez et al., 2015). Studies of other systems have shown

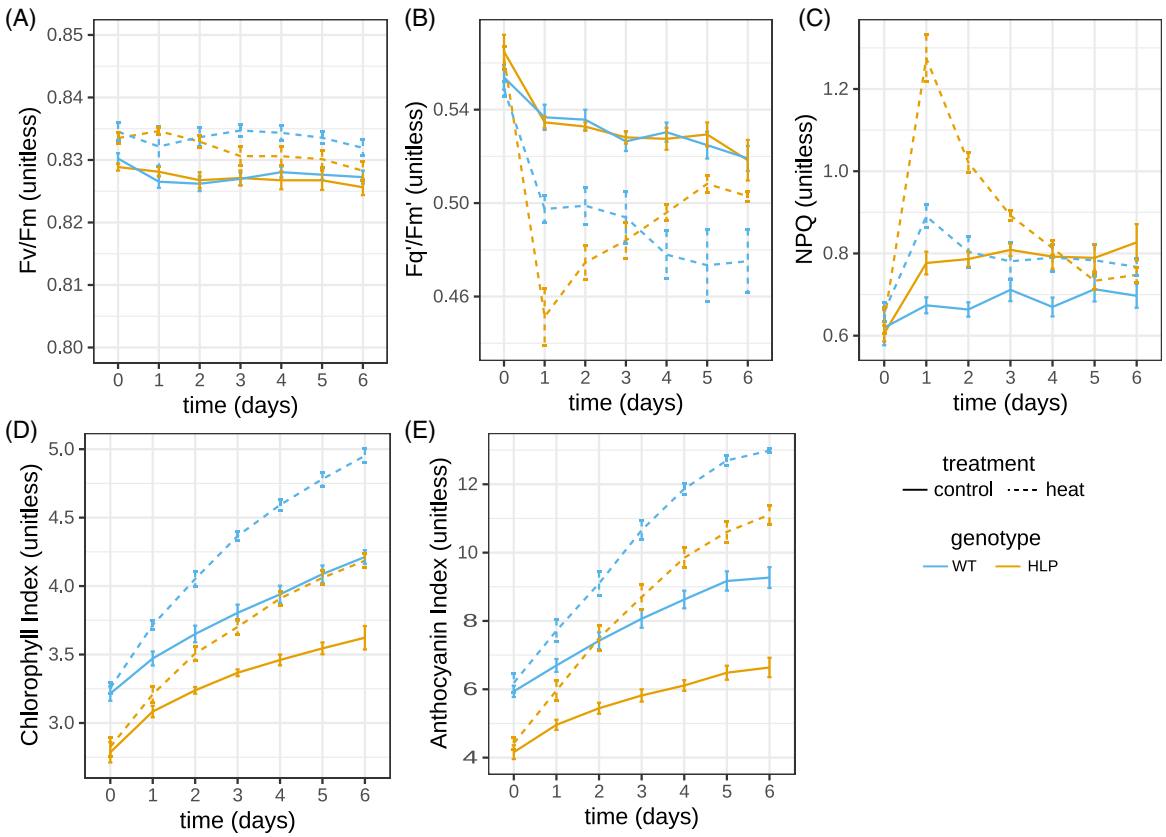

Figure 7. High lipid producing (HLP) had increased NPQ under heat stress as compared with WT.
Photosynthetic efficiency and other stress indices measured using a CropReporter imaging system and image analysis in PlantCV under control (solid line) and heat stress (dotted line) conditions.
(A) Photosystem II maximum quantum efficiency (F_v/F_m).
(B) Photosystem II operating efficiency (F'_q/F'_m).
(C) Non-photochemical quenching (NPQ).
(D) Anthocyanin index.
(E) Chlorophyll index. $n = 4$ plants per genotype and treatment.

significant reductions in F_v/F_m due to abiotic stress over the course of minutes to hours (Mathur et al., 2014) but those studies have not considered long-term exposure to stress that was tested here. F_v/F_m was slightly increased in high temperature for both genotypes, including at Day 0 in which the plants had not yet started stress treatment; while statistically significant ($P < 0.0001$, Days 0–5), the difference was less than 1% of control value and within the range of what is reported for "healthy" tissue, typically ~0.8 (Murchie & Lawson, 2013). The observed minor difference between control and high temperature at Day 0 may be due to other minor differences between the two growth chambers; there were no significant differences due to stress treatment at Day 0 for F'_q/F'_m, NPQ, anthocyanin index, or chlorophyll index.

F'_q/F'_m was significantly decreased due to high temperature in both genotypes on Days 1–6, suggesting high temperature significantly affected the light reactions of photosynthesis, as expected ($P < 0.01$, Figure 7B). Interestingly, HLP plants decreased 15% at Day 1, while WT plants only decreased 7% ($P < 0.0001$ between genotypes). HLP recovered to control levels by Day 6 when F'_q/F'_m was no longer significantly different between control and high temperature HLP plants ($P > 0.01$). While WT had a smaller change on Day 1 than HLP, F'_q/F'_m steadily decreased and remained below control samples at Day 6 ($P < 0.0001$). This suggests that while HLP had a more severe initial response to high temperature, operating efficiency of photosystem II recovered more quickly than WT to return to control levels.

While high temperature initially increased NPQ in both genotypes, the response was genotype-dependent, similar to F'_q/F'_m. After 1 day of high temperatures, HLP had a 64% increase in NPQ due to treatment, while WT had only a 32% increase (Figure 7C). NPQ returned to control levels faster in HLP than WT, as well; NPQ was significantly greater in heat stress at Days 1 and 2 for HLP, while

it remained greater in WT at Days 1, 2, 3, and 4 before returning to control levels ($P < 0.01$, Figure 7B). These data suggest a much greater increase in NPQ in HLP than WT due to heat stress, but a quicker return to baseline, similar to the observed relationship of F_q'/F_m'. It is unclear whether this sharp increase in NPQ and decrease in F_q'/F_m' in HLP plants was due to increased leaf temperature (a result of decreased stomatal aperture), or another unknown effect of excessive leaf oil in HLP. Because NPQ and F_q'/F_m' are related measurements that use some of the same data in their calculations (i.e., light-adapted measurement of Fm′), it is unsurprising the two measurements show similar relationships.

As an initial observation, 30 TEM images from one plant per genotype and treatment were assessed for chloroplast size, and plastoglobulii number and size, and starch granule size after 2 days of heat stress, when the difference between control and high temperature was greatest for NPQ and F_q'/F_m' (Figure S9). Under high temperature conditions, there was no statistically significant difference in chloroplast area, plastoglobule size or number, or starch area between the genotypes (Figure S9). Interestingly, under control conditions, HLP chloroplasts, starch, and plastoglobulii were larger than WT, but WT had a greater number of plastoglobulii ($P < 0.01$, Figure S9). Both genotypes had significantly less starch area due to high temperature treatment, but HLP also had reduced chloroplast area and number of plastoglobulii ($P < 0.01$, Figure S9). While these results are purely observational due to having a single plant per genotype and treatment, they suggest possible changes in chloroplast and plastoglobulii structure due to temperature are unique between genotypes, and may explain observed differences in NPQ and F_q'/F_m'.

Another measure of plant stress responses are chlorophyll and anthocyanin indices. HLP plants had significant reduction in both indices compared with WT at each timepoint, within each treatment ($P < 0.0001$, comparing genotypes within each day) (Figure 7D,E). High temperature conditions significantly increased both indices compared with control in both genotypes at 1 day of high temperature and beyond ($P < 0.0001$, comparing treatments within each day after Day 0) (Figure 7D,E). The change in chlorophyll index due to high temperature was similar for both genotypes, despite a higher starting index for WT. On Day 6, WT and HLP chlorophyll indices were 18% and 16% greater in high temperature than control, respectively (Figure 6D). While high temperature treatment also increased anthocyanin index in both genotypes, HLP was more significantly affected; on Day 6 of treatment, HLP had a 67% increase in anthocyanin index due to temperature, while WT had only 40% increase. Both were significantly greater than control temperatures ($P < 0.05$, Figure 7E). Whether this was a direct effect of high temperature on photosynthetic apparatuses, or through changes in membrane and oil-body lipids, is unclear. These data, in combination with measures of plant biomass, demonstrated that the HLP response to high temperature conditions was different from WT, and the response to stress for a particular genotype was unique by some measures (NPQ, F_q'/F_m', anthocyanin index, and water content) but not others (Fv/Fm, chlorophyll index, dry plant biomass).

HLP tobacco had significant lipid droplets in guard cells

Previous research used confocal microscopy to investigate leaf cross-sections, demonstrating the increased leaf lipids in HLP are abundant in the leaf mesophyll (Chu et al., 2022; Vanhercke et al., 2017). However, from this vantage point, phenotypes of the stomata and guard cells cannot be observed. To better understand why HLP plants have changes in stomatal aperture, lipid content was imaged using confocal microscopy from the abaxial side of the leaf rather than a cross section. While small lipid droplets were present in the WT stomatal guard cells and epidermis, large lipid droplets were present in the HLP guard cells under both control and after 7 days of treatment (representative control images in Figure 8A–D, complete dataset available on Zenodo, https://zenodo.org/records/10711864). In addition, while HLP oil appeared to form spherical droplets, it did not "line" the stomatal opening as in WT (Figure 8C,D).

HLP stoma had significantly more oil than WT in control and high temperature conditions, measured as the area of green pixels per stoma ($P < 0.0001$, Figure 8E). High temperature significantly decreased guard cell oil in HLP by 22% ($P < 0.0001$, Figure 8E). WT guard cell oil was reduced 18% due to high temperatures ($P < 0.05$) and the absolute reduction was much less than HLP given that WT had much lower control levels (Figure 8E). These data suggest a previously unknown location of high oil in HLP guard cells, as well as a reduction in this oil due to high temperature conditions.

We suggest the observed significant reduction in stomatal aperture may have been a result of the presence of excessive oil bodies in HLP stomatal guard cells, which likely impact stomatal aperture. Previous research has shown that when *A. thaliana* lines have disrupted TAG breakdown, the plants have reduced stomatal conductance, and that TAG is a necessary energy source for ATP production to provide energy for guard cell movement to open stomata (Lawson & Matthews, 2020; McLachlan et al., 2016). Given that these lines were engineered to prevent TAG breakdown (Vanhercke et al., 2017), specifically through the expression of oleosin genes that package oil bodies, we hypothesize that TAG may be less available for energy production. An alternative hypothesis is that the physical presence of the large oil bodies restricts changes in the guard cells. It is also possible that changes in

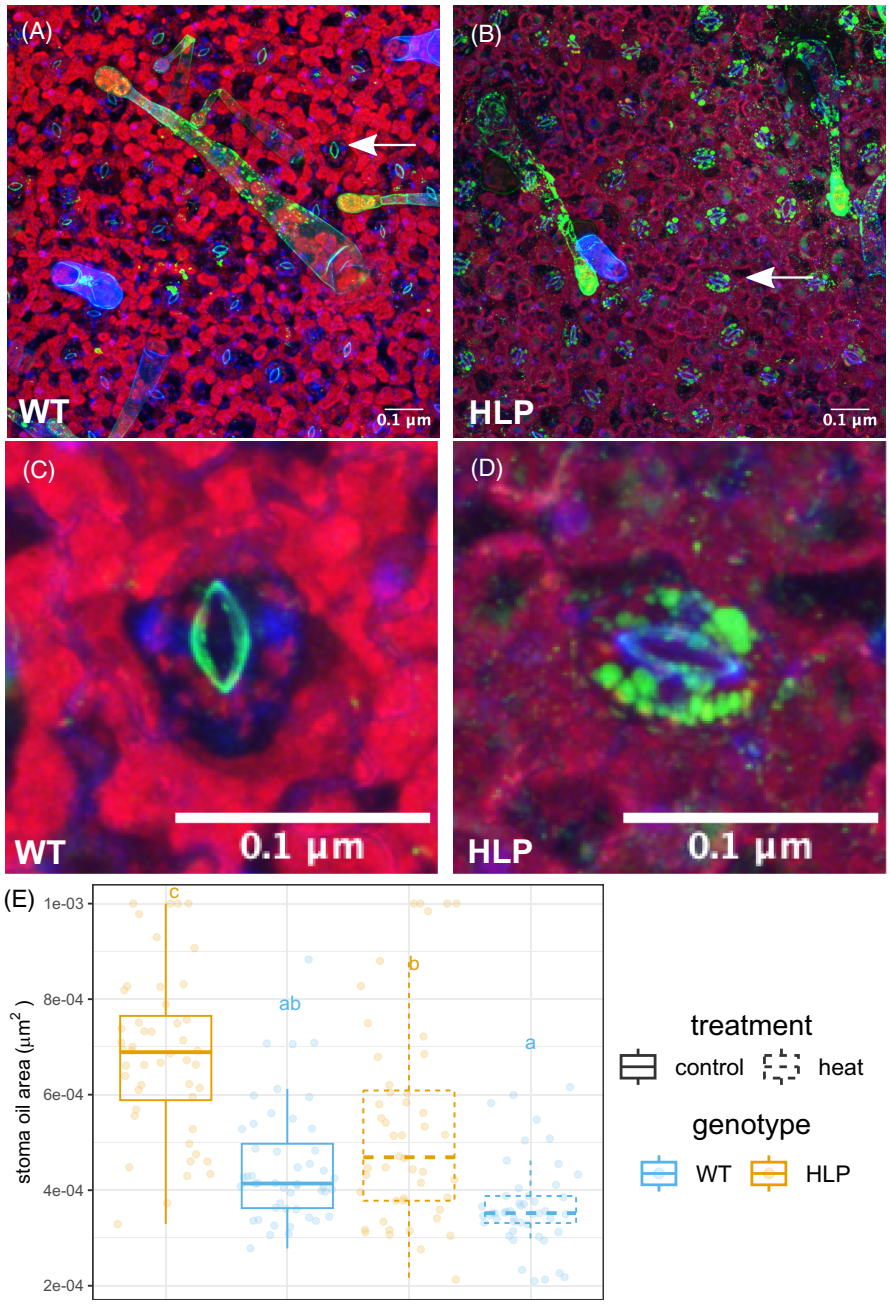

Figure 8. High lipid producing (HLP) had excessive oil droplets in stomatal guard cells.
Representative confocal microscopy images, shown as focused Z-stack, of tobacco leaf tissue fixed in paraformaldehyde.
WT (A, C) and HLP (B, D) are shown; white arrows show a representative stoma that are shown in closer view in (C, D). Red = chlorophyll autofluorescence. Blue = cell wall autofluorescence. Green = lipids stained with BODIPY™ 493/503.
(E) Quantification of area of BODIPY per stoma. Letters represent significantly different groups ($P < 0.05$, ANOVA with LSMEANS *post hoc* test), $n = 48$ (four plants per genotype and treatment, four images per plant, three stoma per image).

signaling because of the genetic modification, specifically transcription factors WRI1 and LEC2, may be influencing guard cell action. Given that LEC2, specifically, is involved in seed development and maturation, it is possible that it is influencing abscisic acid signaling, which is an important hormone in guard cell movement (Andrianov et al., 2010; Liang et al., 2024; Stone et al., 2008; Toh et al., 2018). However, there are no direct reports on the effects of these specific modifications and stomatal conductance.

HLP oil levels were negatively impacted by high temperature conditions

Given the importance of lipids in membrane modifications under temperature stress, and the results of the stoma oil analysis, we sought to understand possible differential impacts of high temperature on leaf lipid accumulation in HLP compared with WT plants. Because oil is the desirable product from HLP plants, assessing the effect of high temperature on oil levels is also critical to understanding the impact of the environment on the product yield. Total lipid content was assessed by derivatization to fatty acid methyl esters (FAMEs). HLP plants had significantly more total FAMEs than WT in all conditions ($P < 0.05$, Figure 9A). High temperature conditions had no effect on WT FAMEs levels (Figure 9A), but significantly reduced HLP total FAMEs accumulation ($P < 0.05$, Figure 9A). FAMEs decreased 31.8% within 2 days of high temperature in HLP plants, and by the end of the 7 day time course had decreased 54.6% ($P < 0.05$, Figure 9A). Whether the reduction in oil in HLP due to temperature was a consequence of reduced synthesis, increased turnover, or a combination of both effects is unknown.

Overall, the high temperature conditions did not substantially affect the total lipid amount in WT (Figure 9A); however, the composition of total lipids was altered (Figures S3 and S4). The most significant changes included reductions in 16:3 and 18:3 in WT FAMEs at Day 7 on a weight percent basis ($P < 0.05$, Figure S4). HLP showed a different relationship: 18:1 was decreased and 18:3 was increased, the reverse of WT ($P < 0.05$, Figure S4).

Shifts in total FAMEs composition can be obscured by the differential accumulation of storage lipids and membrane lipids during the high temperature stress. Therefore, the total lipid extracts were separated into polar and neutral fractions for FAMEs analysis of membrane and storage lipids, respectively (Figure 9B,C). In the WT polar fraction, the amount of FAMEs by mass was similar between temperature treatments with the greatest difference at Day 7 ($P < 0.05$ at Day 7, Figure 9B). Polar lipid composition changed throughout the time course, as well; increases in 18:0, 18:1, and 18:2 (more saturated) fatty acids by weight percent were partially offset by decreases in 16:3 and 18:3 (more unsaturated) fatty acids (Figure S6). The amount of polar lipids did not change with temperature in HLP (Figure 9B); however, the composition did change similar to WT (Figure S6).

While the polar lipids (i.e., membrane lipids) did not change in HLP, the neutral lipids fraction (i.e., storage lipids) was significantly reduced due to high temperature ($P < 0.05$, Figure 9C). The changes in HLP neutral lipids were driven by increases in 18:0 and decreases in 18:1 on a weight percent basis ($P < 0.05$, Figure S8). In contrast, the WT neutral lipid fraction did not change with temperature, and had only modest changes in composition (Figure 9C, Figure S8).

Ultimately, the decrease in total lipid mass in HLP (Figure 9A) was due to a reduction in the stored leaf oil (neutral lipids), not changes in total membrane lipids (polar lipids) (Figure 9B,C). The relationship was reversed

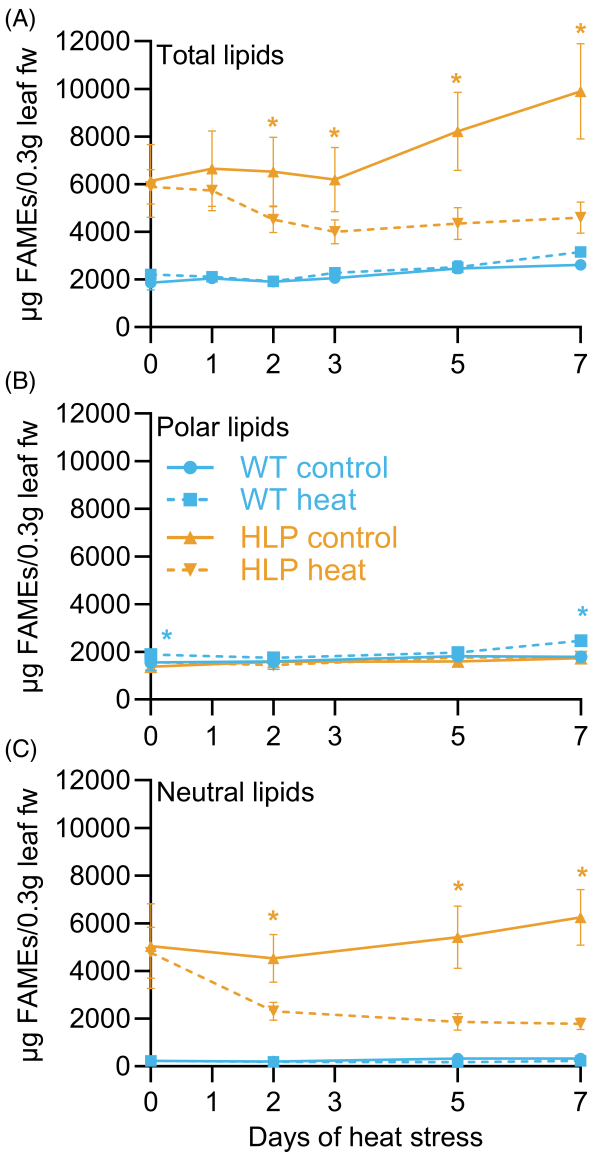

Figure 9. Heat stress reduced total fatty acid methyl esters (FAMEs) in high lipid producing (HLP).
Total fatty acid content measured as FAMEs contained within total lipid extract (A), polar lipid fraction (B), and neutral lipid fraction (C). Controls are solid lines, WT (blue circles) and HLP (orange triangles). High temperature treated are dashed lines WT (blue squares) and HLP (orange upside-down triangles). A blue asterisk indicates significant differences ($P < 0.05$) for comparisons of WT control and WT stress and an orange asterisk for HLP control and HLP stress samples ($P < 0.05$). Data points are the mean and error bars represent standard deviation ($n = 4$), except Day 7 WT and HLP controls ($n = 3$).

in WT, where temperature affected polar lipids (mostly FAME compositions) but not neutral lipids. The polar FAMEs composition profile for WT and HLP polar lipids corresponds to the classical model of heat stress-induced polar lipid remodeling to provide enhanced thermotolerance for the photosynthetic membranes, which includes decreased highly polyunsaturated fatty acids (16:3 and 18:3) with concurrent increases in less unsaturated fatty acids (16:0, 18:1, and 18:2) (Higashi et al., 2015; Routaboul et al., 2012; Shiva et al., 2020). Heat stress-induced lipid remodeling is a dynamic process that involves the reduction in polyunsaturated fatty acids (16:3 and 18:3) in chloroplast lipids (MGDG and DGDG) and the incorporation of more saturated fatty acids to restore membrane stability during temperature stress. Many possible polar lipid lipases can accomplish this remodeling. For example, Heat Inducible Lipase1 (HIL1) specifically liberates 18:3 from MGDG during high temperature conditions (Higashi et al., 2018; Wang et al., 2019). However, the mechanisms of the abundant TAG turnover in HLP during heat stress are not immediately clear. In WT plants, fatty acids released from chloroplast membrane lipids during heat stress are transiently incorporated into low levels of TAG prior to turnover through fatty acid beta-oxidation (Korte et al., 2023). The TAG turnover is likely caused by the TAG lipase Sugar-dependent 1 (SDP1) (Azeez et al., 2022; Aznar-Moreno et al., 2022; Eastmond, 2006). SDP1 expression has also been shown to increase in Arabidopsis leaves and tobacco pollen tubes under heat stress (Higashi et al., 2015; Krawczyk et al., 2022). Therefore, the large reduction in HLP accumulated TAG during heat stress may be due to activation of the endogenous chloroplast membrane lipid remodeling and fatty acid turnover mechanisms.

In conclusion, HLP plants had reduced stomatal conductance, which we hypothesize to be a result of excessive, large oil bodies in HLP stomatal guard cells. This reduced conductance led to increased leaf temperatures, reduced carbon assimilation, and reduced transpiration compared with WT plants. Under high temperature conditions, this increase in leaf temperature was more pronounced. While reduced stomatal conductance may be a benefit under water deficit conditions, the total impact needs to be considered for maintaining plant health and oil yield (Faralli et al., 2019; Verslues et al., 2022). Of course, all results here are valid within the environmental conditions and plant developmental stage tested – changes in temperature, day length, light intensity, fertilizer regime, and other factors may affect lipid production and responses to stress in different ways than those observed here. As future biofuel crops are developed, they must be investigated in the context of future environmental stressors and evaluated for oil yield under different conditions. Here, we show that the oil results in both a modified stress response, and that the stress reduces the overall oil content of the leaves. Nonetheless, it is noteworthy that even under the high temperature conditions, HLP dramatically outperformed WT as a plant for biofuel production, providing a measure of support for next generation engineered plants.

MATERIALS AND METHODS

Plant growth

HLP and WT (Wisconsin 38) tobacco (*N. tabacum*) were provided by CSIRO (Commonwealth Scientific and Industrial Research Organization) (Vanhercke et al., 2017). All plants were grown at the Donald Danforth Plant Science Center in St. Louis, MO, USA. Seed were germinated in Berger BM7 35% Bark HLP soil mix (pH 5.5–6.5) in greenhouse conditions (27°C day/23°C night, 16 h/8 h light/dark, 60–90% relative humidity) in a plug tray with a plastic humidity dome covering; HLP seeds were planted 2 days prior to WT so that all seed germinated on the same day; age of plant is subsequently referred to as the day WT was planted, and thus, HLP plants were always planted 2 days prior. Seedlings were transplanted 2 weeks after sowing into Berger BM7 35% Bark HLP soil mix (pH 5.5–6.5) in 1.07 L square plastic pots with drainage holes and grown at 28°C day/22°C night, 40–50% relative humidity, 14 h day/10 h night in a greenhouse. Supplemental LED lighting was activated when light levels were below 500 $\mu mol\ m^{-2}\ sec^{-1}$. After transplanting, plants were watered with fertilizer water containing 200 ppm Jacks 15-16-17 N–P–K Peat-Lite fertilizer three times per week, and otherwise watered with non-fertilizer water.

Plants were moved to Conviron (Winnipeg, Manitoba, Canada) growth chambers with halogen lights (model PGCFLEX) at 37 days after planting WT and watered using bottom-watering trays and fertilizer water (Jacks 15-5-15 N–P–K Ca–Mg, 1.4–1.6 EC) on weekdays and RO water on weekends to ensure plants were never water stressed. Control conditions were set to 28°C day/18°C night, 12 h/12 h light/dark, 400 $\mu mol\ m^{-2}\ sec^{-1}$, and 60% constant relative humidity; ambient CO_2 was measured to be 475 ppm. Plants were left in control conditions in the growth chambers for 5 days prior to any treatment to ensure acclimation from the greenhouse to the growth chamber prior to the start of the stress application. Given that HLP were slightly smaller than WT, they likely received less light than WT plants, whose top leaves are closer to the light source; to address this limitation plants were spaced sufficiently to avoid shading. The two genotypes were grown in the same chamber to avoid chamber to chamber variation.

For high temperatures, conditions were maintained except temperatures were set to 42°C day/32°C night, and temperature stress began 1 h after dawn, 42 days after planting WT. Four biological replicates were used for all measurements unless otherwise noted. Plant thermal imaging maintained the same conditions in a Conviron walk-in growth chamber (model BDW80), except lights were kept constant for 48 h to maintain camera focus, LEDs were used instead of halogen bulbs, and high temperature was 39°C day/29°C night due to limitations of the growth chamber temperature maximum. Measurements on the DiTech Plantarray used a high temperature treatment of 38°C day/28°C night in a Conviron walk-in growth chamber (model BDW80) with LED lights, with high temperature beginning 35 days after WT planting, due to limitations on the chamber and plant size maximums. In particular, plants must be within a certain size window prior to transplanting on the DiTech Plantarray and evaluated within 10 days of loading onto the equipment, and thus could not

be measured at the same 42-day-old start of high temperature stress as the other experiments.

Plant thermal imaging

A FLIR T630sc camera was used to measure plant temperatures, and images were analyzed using PlantCV (Gehan et al., 2017), version 4, to calculate average plant leaf temperature for each individual plant. To this end, the camera was mounted ~2 m above the plants in a walk-in growth chamber for top-down imaging, and soil and area between plants were covered with black cotton fabric. Images were taken every 15 min for 48 h, without opening or disturbing the growth chamber, with temperatures fluctuating for day/night; lights were kept on to maintain the camera focus without disturbance of the chamber, and humidity was kept constant. Genotypes were alternated in a grid to remove possible positional effects in the chamber, and provided enough space to prevent plants from touching or shading each other. Given there was only one camera, control temperature and high temperature experiments were performed separately; plant age was kept the same for both control and high temperature (39°C day/29°C night) experiments (i.e., beginning 42 days after planting of WT).

To analyze plant temperature images in PlantCV, RGB (red green blue) and thermal images taken on the same camera were registered for precise image alignment. Next, the RGB image was masked using a binary threshold to segment only the plant tissue, and a region of interest combined with object identification was used to isolate only individual plants in each mask. Then, the mask was applied to the registered thermal image to calculate the average plant temperature, as well as a histogram of pixel temperatures for each plant. A PlantCV workflow was used to analyze the images in parallel. A tutorial is available on GitHub: https://github.com/danforthcenter/plantcv-tutorial-thermal?tab=readme-ov-file (Acosta-Gamboa et al., 2024). Scripts for this project are available at https://github.com/danforthcenter/tobacco-heat-paper. Raw image data are available on Zenodo, https://zenodo.org/records/10711864.

Stomatal aperture measurements

To measure stomatal number and aperture, leaf impressions were made using silicone rubber, as previously described (Weyers & Johansen, 1985). First, approximately equal amounts of silicone rubber components [Picodent(r) Twinsil] were mixed using a metal spatula in a plastic petri dish and set for 4 min before careful application to a 1 cm^2 area on the underside of the topmost fully expanded leaf while the plants were inside the growth chamber. Application was done to control and high temperature-treated plants 24 h after the start of high temperature (42°C day/32°C). After 10 min to allow for solidification of the rubber, impressions were peeled using forceps, avoiding any leaf damage, and painted immediately with clear nail polish. The nail polish was peeled the day before imaging using forceps and mounted on a slide under a coverslip. Nail polish was imaged using Nikon E800 NiE Widefield Epifluorescence Microscope, 20× objective using brightfield imaging. Images were taken as Z-stacks, 0.9 μm step size, then auto-projected for a 2D image and saved as a .png file.

Microscopy images were analyzed using PlantCV (Gehan et al., 2017), version 4. In short, images were masked to obtain the center of the stoma (dark), and a point-and-click method was used to select only the stomata and remove noise. The morphology package was then used to calculate the number of stomata and the area of the aperture. A limitation of this method is that it does not provide the width and length of stomata, or measurements of the guard cells themselves; instead, it provides the aperture area (a result of length and width). A tutorial is available on GitHub: https://github.com/danforthcenter/plantcv-stomata-tutorial-pcv4 (Murphy, 2024). Scripts for this project are available at https://github.com/danforthcenter/tobacco-heat-paper. Raw image data are available on Zenodo, https://zenodo.org/records/10711864.

Photosynthesis and gas exchange

Measurements of photosynthesis were made using an LICOR Li-6800 portable photosynthesis system during the day using a 6 cm^2 aperture. Measurements were only performed on plants in control conditions; measurements of plant responses to high temperature were made by adjusting the Li-6800 leaf chamber temperature, not the temperature of the growth chamber. Unless otherwise specified as a changing variable, flow was set to 500 μmol sec^{-1}, CO_2 reference to 475 ppm (to match ambient chamber conditions), fan speed to 10 000 rpm, leaf vapor-pressure deficit (VPD) to 1.5 kPa, light intensity 400 μmol m^{-2} sec^{-1}, and temperature to the control (28°C). The fluorometer was not turned on. CO_2 and H_2O were matched if greater than 10 min had elapsed since the last matching, or if the change in measurement was greater than 100 ppm for CO_2 or 10 mmol/mol for H_2O. The top-most, fully expanded leaf was clamped and measurements were stabilized (slope of the change in CO_2 and H_2O were less than 0.5, typically 2–5 min). Gas exchange measurements and leaf surface temperature were recorded every 1 min using a program adjusting one of the above variables (either ambient leaf chamber temperature or CO_2 reference); assimilation, stomatal conductance, and internal CO_2 concentrations were calculated as described in the Li-6800 manual and elsewhere (Farquhar & Sharkey, 1982; Long & Bernacchi, 2003; Pons et al., 2009). Measurements adjusting CO_2 reference began 5 h after dawn and lasted 1.5 h to complete all measurements; measurements were conducted 42 days after WT planting. Measurements adjusting leaf chamber temperature began 2.5 h after dawn and lasted 5 h, and were conducted over 2 days (42 or 43 days after planting WT) given the length of time required for each measurement; genotypes were equally spread across both days to avoid confounding variables. Thus, all gas exchange measurements with Li-6800 were conducted during peak day hours to avoid effects of the plant circadian clock confounding the results, given that gas exchange is known to be influenced by the circadian clock (de Dios, 2017).

Plant transpiration rates

Plant transpiration rates were calculated using a plant gravimetric phenotyping system (Plant Di-Tech Plantarray 3.0 lysimeter system) (Dalal et al., 2020) under control growth chamber conditions (see plant growth methods above). Plants were grown as described in plant growth methods, except rather than transplanting to 1.07 L pots, seedlings were transplanted to 0.7 L pots necessary for transplanting in the Plantarray system. Plants were subsequently transplanted to 3.79 L round pots 29 days after WT planting, fit with a fabric bottom inset into a sealed weighing container, and plastic foam cover and shower cap with a hole for the plant stem to prevent evaporation of water from the soil. Thirty-five days after WT planting, high temperature (38°C day/28°C) was applied to one growth chamber containing half of the plants. Each plant was individually weighed every 3 min for 7 days, and watered nightly to saturation by irrigation drip tape (NetBow) with fertilizer water (same concentrations described in plant growth methods above). Daily transpiration was calculated as the grams of water lost (i.e., the reduction in measured weight) each day, beginning 2 h after lights on and ending at lights off (g water/day). Normalized daily transpiration was calculated per plant as the

daily transpiration divided by the shoot wet weight (leaves and stem) measured on the last day (Day 7) of the experiment.

Two hours after dawn on Day 7, leaves were removed from the stems of each plant and laid on a black fabric (without touching each other). An image was captured from the top-down view using a Nikon Coolpix digital camera. Leaf number and leaf area was calculated using PlantCV (Gehan et al., 2017). Leaf and stem tissue was then weighed (wet weight), dried at 37°C until tissue was completely dry, and weighed again (dry weight).

Photosynthetic efficiency imaging

Whole-plant photosynthetic efficiency was measured from fluorescence images taken with a CropReporter camera system (PhenoVation) (Baker, 2008; Murchie & Lawson, 2013; Sánchez et al., 2015). Genotype and treatment were alternated with each subsequent plant measured to avoid circadian effects on the measurements. Plants were dark-adapted by placement in a dark room for 30 min, then F_v/F_m was measured using a pulse of bright light and an image of fluorescence at the megapixel scale; camera settings were at factory default, namely that four dark frames were captured with only the red light on, with the highest intensity fluorescence image chosen as Fmin. Data frames were set to 20, with the highest intensity fluorescence image chosen as Fmax; measuring power was 80% for the red light intensity during the induction curve, F_v/F_m shutter to 200 μsec and gain to 400 for the integration time for capturing fluorescence images, and the gain of the analog signal before image digitization. Plants were then immediately light-adapted for 5 min with actinic light power at 50 before a second image, followed by images for color and spectral indices. Spectral images for measuring anthocyanin index were taken using 10 dark frames and 10 data frames, measuring power 30%, and gain of 300 for all channels. The shutter for anthocyanin was 750 μsec, far-red 2787 μsec, and near infrared to 24 032 μsec. Chlorophyll fluorescence was measured using four dark and four data frames, measuring power 50%, gain of 300, and shutter of 800 μsec. Images were processed in PlantCV (Gehan et al., 2017) using the photosynthesis package; the chlorophyll fluorescence image was used to mask the image for only plant pixels, and average F_v/F_m, F'_q/F'_m, NPQ, chlorophyll index, and anthocyanin index were calculated as an average per plant at each timepoint. A tutorial is available on GitHub: https://github.com/danforthcenter/plantcv-tutorial-photosynthesis?tab=readme-ov-file (Schuhl et al., 2024). Scripts for this project are available at https://github.com/danforthcenter/tobacco-heat-paper. Raw image data are available on Zenodo, https://zenodo.org/records/10711864.

Microscopy imaging of lipids

Leaf samples analyzed for lipid content were taken from the topmost, fully expanded leaf after 7 days of control or high temperature (42°C day/32°C night) conditions; final plant age at sampling was 49 days after planting for WT. Fresh tissue was fixed in 4% paraformaldehyde in phosphate buffer saline (PBS) for a minimum of 3 days, then stored covered in foil at 4°C. After 3 or 4 days, leaf samples were syringe infiltrated using BODIPY™ 493/503 (final concentration of 4 μg ml^{-1} in 50 mM PIPES buffer) for 24 h at 4°C prior to imaging (Vanhercke et al., 2017). Leaf samples were subsequently removed from the stain and mounted in water on a slide using a 22 mm glass coverslip. Samples were imaged using Leica SPX-8 confocal microscope with the following settings: 20× HC PLAN APO (0.70 numerical aperture) objective lens, pinhole set to 1 Airy Unit, 1024 × 1024 pixel image dimensions, 566 nm *x*, *y* pixel size, 1.0 zoom, 488 nm excitation and 500–550 nm emission for BODIPY™-labeled lipid droplets (green), 649 nm excitation and 659–779 nm emission for chlorophyll autofluorescence (red), and 405 nm excitation and 415–500 nm emission for cell wall autofluorescence (blue) using the hybrid detector (HyD) (Chu et al., 2022). Z-stacks were acquired with a step size of 2.36 μm from the upper visible trichomes into the mesophyll as deep as would focus clearly. 3D stacks were rendered as maximum intensity projections and analyzed using the Leica LAS AF Lite software.

Oil levels in stomata were quantified by analyzing the Z-stack of each image in Fiji. First, the color channels were split to only analyze the green channel (BODIPY™, per the imaging settings). Regions of interest (ROI) were drawn around at least three stoma per image, Four images per plant, and four plants per genotype and treatment combination. Each circular ROI was manually drawn around representative stomata, and the green pixel area above an automatic threshold (method = Default/Otsu) was measured with the Fiji measurement tool.

Leaf lipid extractions

Leaf samples were taken for plants at dawn daily for 7 days of high temperature (42°C day/32°C night) and a Day 0 timepoint. Plants were used in the same experiment as the fluorescence imaging, but separate plants were used for leaf lipid extractions to prevent leaf damage from affecting the fluorescence imaging measurements. Whole leaf disks (0.635 cm diameter) were collected with a tissue punch (MIDCO Global, St. Louis, MO, USA) into 2.0 ml plastic, screw-top tubes and flash frozen in liquid N_2. Four to six 2.4 mm ceramic beads and 1 ml of preheated (85°C) isopropanol were added to the frozen tissue and heated at 85°C for 10–15 min to inhibit lipid degradation. After heating, samples were cooled to room temperature and homogenized using a bead mill three times for 20 sec each, with 20 sec between each homogenization. Samples were then centrifuged at 21 000 ***g*** for 10 min and supernatant was transferred to an 8 ml glass tube. 1.5 ml of chloroform was added to the original sample and homogenization was repeated. Supernatants were combined, and the process of adding chloroform, homogenizing, and combining all supernatants was repeated to extract neutral lipids. Next, 1.5 ml of 5/5/1 chloroform/methanol/water was added to the original sample, homogenized as described, added to the supernatant collection, and repeated once more with the same solvent ratio. The combined supernatants were then adjusted to a ratio of 2/1/0.8 chloroform/methanol/water for phase separation. The supernatant's lower organic phase containing lipids was transferred to a new 8 ml glass tube. 0.5 ml chloroform was added to the remaining liquids in the supernatant sample, mixed, and the lower organic phase was again removed and added to the first transfer volume. The organic phase was concentrated under stream of N_2 and resuspended in 0.5 ml toluene with 0.001% butylated hydroxytoluene. An aliquot of 1/10 total volume was added to a new 8 ml glass tube with 40 μg 17:0 TAG in 1 ml of 2.5% sulfuric acid in methanol (v/v) and heated for 1 h in an 85°C water bath to convert lipids in the organic phase to fatty acid methyl esters (FAMEs). After cooling the tube containing the FAMEs to room temperature, 200 μl hexanes and 1.5 ml 0.89% potassium chloride (w/v) was added, vigorously shook by hand, vortexed, and centrifuged for 1 min at 500 ***g*** to force phase separation. The upper hexanes phase containing the FAMEs was removed, concentrated under N_2, and resuspended in 0.2 ml hexanes for quantification via gas chromatography with flame ionization detection (GC-FID) on Restek HeavyWAX column (30 m, 0.25 mm inner diameter, 0.25 mm film thickness). Conditions included a 5 μl injection, 1/40 split ratio, and 0.9 ml min^{-1} helium flow rate. Heating conditions were 170°C ramped at 10°C min^{-1} to 230°C, then held 5 min.

FAMEs data were normalized to total lipid extract volume (0.5 ml). For lipid fraction separation, solid-phase extraction (SPE) was performed as previously described with the modification of using only chloroform for neutral lipid collection and 5/5/1 methanol/chloroform/water for the polar lipid collection (Kim & Salem, 1990). After concentrating lipids under stream of N_2, FAMEs analysis was performed as described for total lipid extract. FAMEs derived from the total lipid extract were analyzed for Days 0, 1, 2, 3, 5, and 7, while polar and neutral lipid fractions were analyzed for Days 0, 2, 5, and 7. Two-way analysis of variance (ANOVA) followed by a Fisher's Least Squared Difference (LSD) *post hoc* test with no correction for multiple comparisons was performed using GraphPad Prism version 9.5.1 (528) for MacOS, GraphPad Software, San Diego, CA, USA, www.graphpad.com.

Transmission electron microscopy

Plants for TEM analysis were grown as described above in plant growth methods. After 48 h of heat stress (42°C day/32°C night), the topmost expanded leaf was sampled with a tissue punch (MIDCO Global). Tobacco leaf pieces were placed in tissue cassettes and submerged in a freshly prepared primary fixative solution of 2% paraformaldehyde, 2% glutaraldehyde, 0.01% Tween20 and 0.05% malachite green in 0.1 M sodium cacodylate buffer. The leaf tissues in cassettes were vacuum infiltrated for 30 min to allow the primary fixative to infiltrate into the leaf tissues. Subsequently, the tissue cassettes in the primary fixative were subjected to 2 h of shaking at room temperature (on a benchtop shaker), followed by overnight incubation at 4°C as described previously (Wickramanayake & Czymmek, 2023). The leaf pieces were transferred to 4 ml glass vials and rinsed five times (10 min changes) in 0.1 M sodium cacodylate buffer.

Then, 2 ml of 2% aqueous osmium tetroxide was added and kept for 4 h at room temperature, followed by rinsing three times, 15 min each with distilled water. For *en bloc* staining of uranyl acetate (UA), 1 ml of 1% aqueous UA was added. The vials were placed at 4°C overnight, then incubated in the oven at 50°C for 2 h. The vials were allowed to cool to room temperature, then rinsed with distilled water three times, 15 min each. For *en bloc* lead staining, lead aspartate solution was freshly prepared by dissolving 0.04 g L-aspartic acid and 0.066 g lead nitrate in 10 ml distilled water and adjusting the pH to 5.5 with 1 M NaOH. Two millilitre of lead aspartate was added to the vials, incubated at 50°C for 2 h. Samples were rinsed three times for 15 min each with distilled water and 25% cold acetone in water was added overnight. Dehydration continued using a graded cold acetone series of 50, 75, 95, 2 × 100% on a shaker at room temperature with 30 min for each change. Next, two changes of propylene oxide (30 min each) were carried out to ensure consistent resin infiltration in leaf tissues.

The embedding resin used was a hard formulation of Quetol 651/NSA. Resin infiltration steps were conducted at room temperature on a benchtop shaker, with a 6 h interval between changes. Initial resin changes involved using 3:1, 2:1, 1:1, 1:2 and 1:3 propylene oxide:quetol without the accelerator (DMP30). Subsequently, two changes of 100% Quetol without DMP30 and two changes of 100% Quetol with DMP30 were performed. Following resin infiltration, the leaf pieces were embedded in an embedding mold at 60°C for 48 h. All solution exchanges were performed in a fume hood, and liquid and solid waste were discarded according to local regulations. Finally, embedded samples were trimmed with a razor blade and sectioned with a diamond knife using a Leica Ultracut UCT ultramicrotome. The sections (70 nm) were collected onto gold slot grids and imaged on a Talos L120C at 120 kV.

Measurements of chloroplasts and their internal structures were taken from TEM images using Maps offline viewer and Fiji software. Maps offline viewer was utilized to collect 31 (for WT) or 30 (for HLP) zoomed-in images, each containing at least one chloroplast, from one plant per genotype and treatment (sample image in Figure S9); all sub-images were selected using the same zoom level. Sub-images were selected by two requirements: at least one chloroplast must fit completely in the image, and at least 10 thylakoid grana must have been visible and distinguishable inside the chloroplast. Chloroplast size, starch size, and plastoglobulii number and size were then analyzed for the sub-images using Fiji. Chloroplast size and starch size were measured using the ROI manager and the polygon selection tool; plastoglobulii diameter was measured using the line tool.

Statistical analysis

All statistical analyses were performed using R (version 2024.04.2+764). When determining significant factors, a linear model was made using the LSMEANS package, followed by subsequent ANOVA (Lenth, 2016). Unless otherwise noted, data were analyzed using a two-way ANOVA for the significance of genotype, treatment, and time point, followed by a post hoc test to compare estimated marginal means (LSMEANS) to determine which sample types were significantly different from others. Means are reported in text with standard error. Plots were made using ggplot2 package (v.3.5.0) in R. Jupyter notebooks associated with PlantCV analyses and R scripts associated with this manuscript are available on Github (https://github.com/danforthcenter/tobacco-heat-paper).

AUTHOR CONTRIBUTIONS

DKA, MAG, PDB, BSJ and KMM designed experiments. KMM and BSJ performed experiments and data analysis. KJC designed and aided KMM in confocal and brightfield microscopy experiments and advised TEM experiments. JW performed TEM experiments, and KG-O and SK performed data analysis of TEM images. HS wrote scripts for thermal image analysis. CH assisted with LiCOR experiments and stomata image analysis. AF and AB analyzed confocal images for oil content. KMM wrote the article with contributions from all authors.

ACKNOWLEDGEMENTS

Thank you to Xue-Rong Zhou CSIRO (Commonwealth Scientific and Industrial Research Organization) for supplying WT and HLP tobacco seeds used in these experiments. We thank Kevin Reilly and Kris Haines (Integrated Plant Growth Facility, Donald Danforth Plant Science Center, RRID:SCR_024902) for their expertise and assistance in plant growth, and Leonardo Chavez and Joseph Duenwald (Phenotyping Core, Donald Danforth Plant Science Center, RRID:SCR_019049) for their assistance with the DiTech Plantarray. Thank you to Kevin Chu for his advice on experimental design. We thank the Anastasiya Klebanovych for imaging support and the Advanced Bioimaging Laboratory (Donald Danforth Plant Science Center, RRID:SCR_018951) and assistance in microscopy protocols, and for the usage of the ThermoFisher Scientific Talos L120C TEM acquired through generous donor support to the Donald Danforth Plant Science Center, and usage of the Leica SP8-X confocal microscope acquired through an National Science Foundation Major Research Instrumentation grant (DBI-1337680). K.M.M. was supported by a National Science Foundation

Postdoctoral Research Fellowship in Biology (2109387). D.K.A. was supported by the United States Department of Agriculture-Agricultural Research Service. This work was supported by the United States Department of Agriculture-National Institute of Food and Agriculture (2021-67013-33778 to M.A.G., D.K.A., and P.D.B.; 2019-67021-29926 to M.A.G.; and 2022-67021-36467 to M.A.G.), the Hatch Umbrella Project #1015621, the MultiState Project #NC1203, and a Donald Danforth Plant Science Center Enterprise Rent-A-Car Research Institute Grant. C.H. was supported by the National Science Foundation Research Experience for Undergraduates (2050394).

CONFLICT OF INTEREST STATEMENT

The authors declare no conflicts of interest.

DATA AVAILABILITY STATEMENT

The data that support the findings of this study are openly available in GitHub at https://github.com/danforthcenter/tobacco-heat-paper and Zenodo at https://zenodo.org/records/10711864, DOI: 10.5281/zenodo.10711863.

SUPPORTING INFORMATION

Additional Supporting Information may be found in the online version of this article.

Figure S1. Leaf temperature was increased in HLP, measured using LiCOR Li-6800. Leaf temperature measured on the topmost fully expanded leaf under control (28°C), and 24 min after the Li-6800 leaf chamber temperature was increased to heat stress conditions (42°C), measured using a LiCOR Li-6800. $n = 4$ plants per genotype and treatment. $^{*}P < 0.1$.

Figure S2. Internalized versus ambient CO_2 differed by genotype and ambient CO_2 levels. Internalized (Ci) over ambient (Ca) CO_2 levels measured using a LiCOR Li-6800 portable photosynthesis meter under changing Ca levels and under control conditions (28°C). These data were used to construct the A/Ci curve (Figure 4). $^{*}P < 0.1$, $^{**}P < 0.01$, $^{***}P < 0.001$, $^{****}P < 0.0001$.

Figure S3. Total lipid individual fatty acid mass accumulation during heat stress. Total lipid fatty acid content measured in micrograms (μg) FAME for WT and HLP tobacco. Fatty acids represented as number of carbons: number of double bonds (a–i) is 16:0 16:1, 16:1trans3, 16:2, 16:3, 18:0, 18:1, 18:2, and 18:3, respectively. Controls are solid lines, WT (blue circles) and HLP (orange triangles). Heat stress are dashed lines WT (blue squares) and HLP (orange upside-down triangles). A blue asterisk indicates significant differences ($P < 0.05$) for comparisons of WT control and WT stress and a orange asterisk for HLP control and HLP stress samples. Data points are the mean and error bars represent standard deviation ($n = 4$), except Day 7 WT and HLP controls ($n = 3$).

Figure S4. Total lipid individual fatty acid composition changes during heat stress. Total lipid fatty acid composition expressed as the weight percent of total FAMEs (Wt % FAMEs). Fatty acids represented as the number of carbons: number of double bonds (a–i) is 16:0, 16:1, 16:1trans3, 16:2, 16:3, 18:0, 18:1, 18:2, and 18:3, respectively. Controls are solid lines, WT (blue circles) and HLP (orange triangles). High temperature treated are dashed lines WT (blue squares) and HLP (orange upside-down triangles). A blue asterisk indicates significant differences ($P < 0.05$) for comparisons of WT control and WT stress and an orange asterisk for HLP control and HLP stress samples. Data points are the mean and error bars represent standard deviation ($n = 4$), except Day 7 WT and HLP controls ($n = 3$).

Figure S5. Polar lipid fraction individual fatty acid mass accumulation during high temperature stress. Polar lipid fraction fatty acid content measured in micrograms (μg) FAMEs for WT and HLP tobacco. Fatty acids represented as number of carbons: number of double bonds (a–i) is 16:0 16:1, 16:1trans3, 16:2, 16:3, 18:0, 18:1, 18:2, and 18:3, respectively. Controls are solid lines, WT (blue circles) and HLP (orange triangles). High temperature treated are dashed lines WT (blue squares) and HLP (orange upside-down triangles). A blue asterisk indicates significant differences ($P < 0.05$) for comparisons of WT control and WT stress and an orange asterisk for HLP control and HLP stress samples. Data points are the mean and error bars represent standard deviation ($n = 4$), except Day 7 WT and HLP controls ($n = 3$).

Figure S6. Polar lipid fraction individual fatty acid composition changes during heat stress. Polar lipid fraction fatty acid composition expressed as the weight percent of total FAMEs (Wt % FAMEs). Fatty acids represented as number of carbons: number of double bonds (a–i) is 16:0 16:1, 16:1trans3, 16:2, 16:3, 18:0, 18:1, 18:2, and 18:3, respectively. Controls are solid lines, WT (blue circles) and HLP (orange triangles). High temperature treated are dashed lines WT (blue squares) and HLP (orange upside-down triangles). A blue asterisk indicates significant differences ($P < 0.05$) for comparisons of WT control and WT stress and an orange asterisk for HLP control and HLP stress samples. Data points are the mean and error bars represent standard deviation ($n = 4$), except Day 7 WT and HLP controls ($n = 3$).

Figure S7. Neutral lipid fraction individual fatty acid mass accumulation during high temperature stress. Neutral lipid fraction fatty acid content measured in micrograms (μg) FAMEs for WT and HLP tobacco. Fatty acids represented as number of carbons: number of double bonds (a–i) is 16:0 16:1, 16:1trans3, 16:2, 16:3, 18:0, 18:1, 18:2, and 18:3, respectively. Controls are solid lines, WT (blue circles) and HLP (orange triangles). High temperature treated are dashed lines WT (blue squares) and HLP (orange upside-down triangles). A blue asterisk indicates significant differences ($P < 0.05$) for comparisons of WT control and WT stress and an orange asterisk for HLP control and HLP stress samples. Data points are the mean and error bars represent standard deviation ($n = 4$), except Day 7 WT and HLP controls ($n = 3$).

Figure S8. Neutral lipid fraction individual fatty acid composition changes during heat stress. Neutral lipid fraction fatty acid composition expressed as the weight percent of total FAMEs (Wt % FAMEs). Fatty acids represented as number of carbons: number of double bonds (a–i) is 16:0 16:1, 16:1trans3, 16:2, 16:3, 18:0, 18:1, 18:2, and 18:3, respectively. Controls are solid lines, WT (blue circles) and HLP (orange triangles). High temperature treated are dashed lines WT (blue squares) and HLP (orange upside-down triangles). A blue asterisk indicates significant differences ($P < 0.05$) for comparisons of WT control and WT stress and an orange asterisk for HLP control and HLP stress samples. Data points are the mean and error bars represent standard deviation ($n = 4$), except Day 7 WT and HLP controls ($n = 3$).

Figure S9. TEM imaging suggests observational differences in organelle structure due to genotype and treatment. (a) Chloroplast area (nm^2), (b) plastoglobulii diameter (nm), (c) Number of plastoglobulii, (d) starch area (nm^2). Letters represent significant difference by ANOVA ($P < 0.05$). (e) Example TEM image of an HLP plant under heat stress; example starch, chloroplast, and plastoglobulii are annotated. TEM, transmission electron microscopy. Number of plants tested = 1 plant per genotype and treatment. Number of images per plant, $n = 30$ images.

REFERENCES

Acosta-Gamboa, L., **Haley Schuhl, H.** & **Murphy, K.M.** (2024) *danforthcenter/plantcv-tutorial-thermal: plantCV thermal tutorial*. Available from: https://doi.org/10.5281/zenodo.10552709

Allakhverdiev, S.I., **Kreslavski, V.D.**, **Klimov, V.V.**, **Los, D.A.**, **Carpentier, R.** & **Mohanty, P.** (2008) Heat stress: an overview of molecular responses in photosynthesis. *Photosynthesis Research*, **98**(1–3), 541–550. Available from: https://doi.org/10.1007/s11120-008-9331-0

Andrianov, V., **Borisjuk, N.**, **Pogrebnyak, N.**, **Brinker, A.**, **Dixon, J.**, **Spitsin, S.** ***et al.*** (2010) Tobacco as a production platform for biofuel: overexpression of Arabidopsis DGAT and LEC2 genes increases accumulation and shifts the composition of lipids in green biomass. *Plant Biotechnology Journal*, **8**(3), 277–287. Available from: https://doi.org/10.1111/j.1467-7652.2009.00458.x

Azeez, A., **Parchuri, P.** & **Bates, P.D.** (2022) Suppression of *Physaria fendleri* SDP1 increased seed oil and hydroxy fatty acid content while maintaining oil biosynthesis through triacylglycerol remodeling. *Frontiers in Plant Science*, **13**, 931310. Available from: https://doi.org/10.3389/fpls.2022.931310

Aznar-Moreno, J.A., **Mukherjee, T.**, **Morley, S.A.**, **Duressa, D.**, **Kambhampati, S.**, **Chu, K.L.** ***et al.*** (2022) Suppression of SDP1 improves soybean seed composition by increasing oil and reducing undigestible oligosaccharides. *Frontiers in Plant Science*, **13**, 863254. Available from: https://doi.org/10.3389/fpls.2022.863254

Baker, N.R. (2008) Chlorophyll fluorescence: a probe of photosynthesis in vivo. *Annual Review of Plant Biology*, **59**, 89–113. Available from: https://doi.org/10.1146/annurev.arplant.59.032607.092759

Barber, J., **Ford, R.C.**, **Mitchell, R.A.** & **Millner, P.A.** (1984) Chloroplast thylakoid membrane fluidity and its sensitivity to temperature. *Planta*, **161**(4), 375–380. Available from: https://doi.org/10.1007/BF00398729

Bernacchi, C.J., **Pimentel, C.** & **Long, S.P.** (2003) In vivo temperature response functions of parameters required to model RuBP-limited photosynthesis. *Plant, Cell & Environment*, **26**(9), 1419–1430. Available from: https://doi.org/10.1046/j.0016-8025.2003.01050.x

Bernacchi, C.J., **Singsaas, E.L.**, **Pimentel, C.**, **Portis, A.R., Jr.** & **Long, S.P.** (2001) Improved temperature response functions for models of rubisco-limited photosynthesis: in vivo rubisco enzyme kinetics. *Plant, Cell & Environment*, **24**(2), 253–259. Available from: https://doi.org/10.1111/j.1365-3040.2001.00668.x

Bernacchi, C.J., **Portis, A.R.**, **Nakano, H.**, **von Caemmerer, S.** & **Long, S.P.** (2002) Temperature response of mesophyll conductance. Implications for the determination of rubisco enzyme kinetics and for limitations to photosynthesis in vivo. *Plant Physiology*, **130**(4), 1992–1998. Available from: https://doi.org/10.1104/pp.008250

Bita, C.E. & **Gerats, T.** (2013) Plant tolerance to high temperature in a changing environment: scientific fundamentals and production of heat stress-tolerant crops. *Frontiers in Plant Science*, **4**, 273. Available from: https://doi.org/10.3389/fpls.2013.00273

Carlsson, A.S., **Yilmaz, J.L.**, **Green, A.G.**, **Stymne, S.** & **Hofvander, P.** (2011) Replacing fossil oil with fresh oil – with what and for what? *European Journal of Lipid Science and Technology: EJLST*, **113**(7), 812–831. Available from: https://doi.org/10.1002/ejlt.201100032

Casto, A., **Schuhl, H.**, **Schneider, D.**, **Wheeler, J.**, **Gehan, M.** & **Fahlgren, N.** (2021) Analyzing chlorophyll fluorescence images in PlantCV. *Earth and Space Science Open Archive*. Available from: https://doi.org/10.1002/essoar.10508322.2

Chaudhry, S. & **Sidhu, G.P.S.** (2022) Climate change regulated abiotic stress mechanisms in plants: a comprehensive review. *Plant Cell Reports*, **41**(1), 1–31. Available from: https://doi.org/10.1007/s00299-021-02759-5

Chu, K.L., **Koley, S.**, **Jenkins, L.M.**, **Bailey, S.R.**, **Kambhampati, S.**, **Foley, K.** ***et al.*** (2022) Metabolic flux analysis of the non-transitory starch tradeoff for lipid production in mature tobacco leaves. *Metabolic Engineering*, **69**, 231–248. Available from: https://doi.org/10.1016/j.ymben.2021.12.003

Dalal, A., **Shenhar, I.**, **Bourstein, R.**, **Mayo, A.**, **Grunwald, Y.**, **Averbuch, N.** ***et al.*** (2020) A telemetric, gravimetric platform for real-time physiological phenotyping of plant--environment interactions. *JoVE (Journal of Visualized Experiments)*, **162**, e61280.

de Dios, V.R. (2017) Circadian regulation and diurnal variation in gas exchange. *Plant Physiology*, **175**, 3–4. Available from: https://doi.org/10.1104/pp.17.00984

dos Santos, T.B., **Ribas, A.F.**, **de Souza, S.G.H.**, **Budzinski, I.G.F.** & **Domingues, D.S.** (2022) Physiological responses to drought, salinity, and heat stress in plants: a review. *Stress*, **2**(1), 113–135. Available from: https://doi.org/10.3390/stresses2010009

Eastmond, P.J. (2006) SUGAR-DEPENDENT1 encodes a patatin domain triacylglycerol lipase that initiates storage oil breakdown in germinating Arabidopsis seeds. *The Plant Cell*, **18**(3), 665–675. Available from: https://doi.org/10.1105/tpc.105.040543

El-Araby, R. (2024) Biofuel production: exploring renewable energy solutions for a greener future. *Biotechnology for Biofuels and Bioproducts*, **17**(1), 129. Available from: https://doi.org/10.1186/s13068-024-02571-9

Fahlgren, N., **Feldman, M.**, **Gehan, M.A.**, **Wilson, M.S.**, **Shyu, C.**, **Bryant, D.W.** ***et al.*** (2015) A versatile phenotyping system and analytics platform reveals diverse temporal responses to water availability in Setaria. *Molecular Plant*, **8**(10), 1520–1535.

Faralli, M., **Bontempo, L.**, **Bianchedi, P.L.**, **Moser, C.**, **Bertamini, M.**, **Lawson, T.** ***et al.*** (2021) Natural variation in stomatal dynamics drives divergence in heat stress tolerance and contributes to seasonal intrinsic water-use efficiency in *Vitis vinifera* (subsp. *sativa* and *sylvestris*). *Journal of Experimental Botany*, **73**(10), 3238–3250. Available from: https://doi.org/10.1093/jxb/erab552

Faralli, M., **Matthews, J.** & **Lawson, T.** (2019) Exploiting natural variation and genetic manipulation of stomatal conductance for crop improvement. *Current Opinion in Plant Biology*, **49**, 1–7. Available from: https://doi.org/10.1016/j.pbi.2019.01.003

Farquhar, G.D. & **Sharkey, T.D.** (1982) Stomatal conductance and photosynthesis. *Annual Review of Plant Physiology*, **33**(1), 317–345. Available from: https://doi.org/10.1146/annurev.pp.33.060182.001533

Gehan, M.A., **Fahlgren, N.**, **Abbasi, A.**, **Berry, J.C.**, **Callen, S.T.**, **Chavez, L.** ***et al.*** (2017) PlantCV v2: image analysis software for high-throughput plant phenotyping. *PeerJ*, **5**, e4088. Available from: https://doi.org/10.7717/peerj.4088

Hasanuzzaman, M., **Nahar, K.**, **Alam, M.M.**, **Roychowdhury, R.** & **Fujita, M.** (2013) Physiological, biochemical, and molecular mechanisms of heat stress tolerance in plants. *International Journal of Molecular Sciences*, **14**(5), 9643–9684. Available from: https://doi.org/10.3390/ijms14059643

He, M. & **Ding, N.-Z.** (2020) Plant unsaturated fatty acids: multiple roles in stress response. *Frontiers in Plant Science*, **11**, 562785. Available from: https://doi.org/10.3389/fpls.2020.562785

Higashi, Y., **Okazaki, Y.**, **Myouga, F.**, **Shinozaki, K.** & **Saito, K.** (2015) Landscape of the lipidome and transcriptome under heat stress in *Arabidopsis thaliana*. *Scientific Reports*, **5**, 10533. Available from: https://doi.org/10.1038/srep10533

Higashi, Y., **Okazaki, Y.**, **Takano, K.**, **Myouga, F.**, **Shinozaki, K.**, **Knoch, E.** ***et al.*** (2018) HEAT INDUCIBLE LIPASE1 remodels chloroplastic monogalactosyldiacylglycerol by liberating α-linolenic acid in Arabidopsis leaves under heat stress. *The Plant Cell*, **30**(8), 1887–1905. Available from: https://doi.org/10.1105/tpc.18.00347

Hu, S., **Ding, Y.** & **Zhu, C.** (2020) Sensitivity and responses of chloroplasts to heat stress in plants. *Frontiers in Plant Science*, **11**, 375. Available from: https://doi.org/10.3389/fpls.2020.00375

IPCC. (2014) *Climate change 2014 synthesis report*. Geneva, Switzerland: IPCC. Available from: ftp://atitlan.ethz.ch/docs/afischli/for-srinivasan/TS-01978822-Can't%20suppress%20pdf%20indexing%20during%20imports/Attached%20PDFs/Ip096.pdf [Accessed 9th June 2024].

Jagadish, S.V.K., **Way, D.A.** & **Sharkey, T.D.** (2021) Plant heat stress: concepts directing future research. *Plant, Cell & Environment*, **44**(7), 1992–2005. Available from: https://doi.org/10.1111/pce.14050

Johnson, B.S., **Allen, D.K.** & **Bates, P.D.** (2025) Triacylglycerol stability limits futile cycles and inhibition of carbon capture in oil-accumulating leaves. *Plant Physiology*, **197**(2), kiae121. Available from: https://doi.org/10.1093/plphys/kiae121/7618152

Kim, H.Y. & **Salem, N., Jr.** (1990) Separation of lipid classes by solid phase extraction. *Journal of Lipid Research*, **31**(12), 2285–2289. Available from: https://www.ncbi.nlm.nih.gov/pubmed/2090722

Korte, P., **Unzner, A.**, **Damm, T.**, **Berger, S.**, **Krischke, M.** & **Mueller, M.J.** (2023) High triacylglycerol turnover is required for efficient opening of stomata during heat stress in Arabidopsis. *The Plant Journal*, **115**(1), 81–96. Available from: https://doi.org/10.1111/tpj.16210

Krawczyk, H.E., **Rotsch, A.H.**, **Herrfurth, C.**, **Scholz, P.**, **Shomroni, O.**, **Salinas-Riester, G.** ***et al.*** (2022) Heat stress leads to rapid lipid

remodeling and transcriptional adaptations in *Nicotiana tabacum* pollen tubes. *Plant Physiology*, **189**(2), 490–515. Available from: https://doi.org/10.1093/plphys/kiac127

Kusumi, K., **Hirotsuka, S.**, **Kumamaru, T.** & **Iba, K.** (2012) Increased leaf photosynthesis caused by elevated stomatal conductance in a rice mutant deficient in SLAC1, a guard cell anion channel protein. *Journal of Experimental Botany*, **63**(15), 5635–5644. Available from: https://doi.org/10.1093/jxb/ers216

Lawson, T. & **Matthews, J.** (2020) Guard cell metabolism and stomatal function. *Annual Review of Plant Biology*, **71**, 273–302. Available from: https://doi.org/10.1146/annurev-arplant-050718-100251

Lawson, T. & **Vialet-Chabrand, S.** (2019) Speedy stomata, photosynthesis and plant water use efficiency. *The New Phytologist*, **221**(1), 93–98. Available from: https://doi.org/10.1111/nph.15330

Lenth, R.V. (2016) Least-squares means: the R package lsmeans. *Journal of Statistical Software*, **69**, 1–33. Available from: https://doi.org/10.18637/jss.v069.i01

Liang, K., **Chen, Y.**, **Hou, J.**, **Yan, F.** & **Liu, F.** (2024) ABA-mediated stomatal response modulates the effects of drought, salinity and combined stress on tomato plants grown under elevated CO_2. *Environmental and Experimental Botany*, **223**, 105797. Available from: https://doi.org/10.1016/j.envexpbot.2024.105797

Long, S.P. & **Bernacchi, C.J.** (2003) Gas exchange measurements, what can they tell us about the underlying limitations to photosynthesis? Procedures and sources of error. *Journal of Experimental Botany*, **54**(392), 2393–2401. Available from: https://doi.org/10.1093/jxb/erg262

Lu, J., **Xu, Y.**, **Wang, J.**, **Singer, S.D.** & **Chen, G.** (2020) The role of triacylglycerol in plant stress response. *Plants*, **9**(4), 472. Available from: https://doi.org/10.3390/plants9040472

Mathur, S., **Agrawal, D.** & **Jajoo, A.** (2014) Photosynthesis: response to high temperature stress. *Journal of Photochemistry and Photobiology. B, Biology*, **137**, 116–126. Available from: https://doi.org/10.1016/j.jphotobiol.2014.01.010

McLachlan, D.H., **Lan, J.**, **Geilfus, C.-M.**, **Dodd, A.N.**, **Larson, T.**, **Baker, A.** ***et al.*** (2016) The breakdown of stored triacylglycerols is required during light-induced stomatal opening. *Current Biology: CB*, **26**(5), 707–712. Available from: https://doi.org/10.1016/j.cub.2016.01.019

Murakami, Y., **Tsuyama, M.**, **Kobayashi, Y.**, **Kodama, H.** & **Iba, K.** (2000) Trienoic fatty acids and plant tolerance of high temperature. *Science*, **287**(5452), 476–479.

Murchie, E.H. & **Lawson, T.** (2013) Chlorophyll fluorescence analysis: a guide to good practice and understanding some new applications. *Journal of Experimental Botany*, **64**(13), 3983–3998. Available from: https://doi.org/10.1093/jxb/ert208

Murphy, K.M. (2024) *danforthcenter/plantcv-stomata-tutorial-pcv4: plantCV stomata tutorial*. Available from: https://doi.org/10.5281/zenodo.10520121

Pons, T.L., **Flexas, J.**, **von Caemmerer, S.**, **Evans, J.R.**, **Genty, B.**, **Ribas-Carbo, M.** ***et al.*** (2009) Estimating mesophyll conductance to CO_2: methodology, potential errors, and recommendations. *Journal of Experimental Botany*, **60**(8), 2217–2234. Available from: https://doi.org/10.1093/jxb/erp081

Ranawana, S.R.W.M.C.J.K., **Bramley, H.**, **Palta, J.A.** & **Siddique, K.H.M.** (2023) Role of transpiration in regulating leaf temperature and its application in physiological breeding. In: Palta, J.A. (Ed.) *Translating physiological tools to augment crop breeding*. Singapore: Springer Nature Singapore, pp. 91–119. Available from: https://doi.org/10.1007/978-981-19-7498-4_5

Rivero, R.M., **Mittler, R.**, **Blumwald, E.** & **Zandalinas, S.I.** (2022) Developing climate-resilient crops: improving plant tolerance to stress combination. *The Plant Journal: For Cell and Molecular Biology*, **109**(2), 373–389. Available from: https://doi.org/10.1111/tpj.15483

Routaboul, J.-M., **Skidmore, C.**, **Wallis, J.G.** & **Browse, J.** (2012) Arabidopsis mutants reveal that short- and long-term thermotolerance have different requirements for trienoic fatty acids. *Journal of Experimental Botany*, **63**(3), 1435–1443. Available from: https://doi.org/10.1093/jxb/err381

Sadok, W., **Lopez, J.R.** & **Smith, K.P.** (2021) Transpiration increases under high-temperature stress: potential mechanisms, trade-offs and prospects for crop resilience in a warming world. *Plant, Cell & Environment*, **44**(7), 2102–2116. Available from: https://doi.org/10.1111/pce.13970

Sánchez, E.G., **Heuvelink, E.**, **de Gelder, A.** & **Stanghellini, C.** (2015) New non-invasive tools for early plant stress detection. *Procedia Environmental Sciences*, **29**, 249–250. Available from: https://doi.org/10.1016/j.proenv.2015.07.296

Schuhl, H., **Fahlgren, N.** & **Murphy, K.** (2024) *Danforthcenter/plantcv-tutorial-photosynthesis: plantCV photosynthesis tutorial*. Zenodo. Available from: https://doi.org/10.5281/ZENODO.10552703

Shiva, S., **Samarakoon, T.**, **Lowe, K.A.**, **Roach, C.**, **Vu, H.S.**, **Colter, M.** ***et al.*** (2020) Leaf lipid alterations in response to heat stress of *Arabidopsis thaliana*. *Plants*, **9**(7), 845. Available from: https://doi.org/10.3390/plants9070845

Stone, S.L., **Braybrook, S.A.**, **Paula, S.L.**, **Kwong, L.W.**, **Meuser, J.**, **Pelletier, J.** ***et al.*** (2008) Arabidopsis LEAFY COTYLEDON2 induces maturation traits and auxin activity: implications for somatic embryogenesis. *Proceedings of the National Academy of Sciences of the United States of America*, **105**(8), 3151–3156. Available from: https://doi.org/10.1073/pnas.0712364105

Toh, S., **Inoue, S.**, **Toda, Y.**, **Yuki, T.**, **Suzuki, K.**, **Hamamoto, S.** ***et al.*** (2018) Identification and characterization of compounds that affect stomatal movements. *Plant & Cell Physiology*, **59**(8), 1568–1580. Available from: https://doi.org/10.1093/pcp/pcy061

Vanhercke, T., **Divi, U.K.**, **El Tahchy, A.**, **Liu, Q.**, **Mitchell, M.**, **Taylor, M.C.** ***et al.*** (2017) Step changes in leaf oil accumulation via iterative metabolic engineering. *Metabolic Engineering*, **39**, 237–246. Available from: https://doi.org/10.1016/j.ymben.2016.12.007

Vanhercke, T., **El Tahchy, A.**, **Liu, Q.**, **Zhou, X.-R.**, **Shrestha, P.**, **Divi, U.K.** ***et al.*** (2014) Metabolic engineering of biomass for high energy density: oilseed-like triacylglycerol yields from plant leaves. *Plant Biotechnology Journal*, **12**(2), 231–239. Available from: https://doi.org/10.1111/pbi.12131

Verslues, P.E., **Bailey-Serres, J.**, **Brodersen, C.**, **Buckley, T.N.**, **Conti, L.**, **Christmann, A.** ***et al.*** (2022) Burning questions for a warming and changing world: 15 unknowns in plant abiotic stress. *The Plant Cell*, **35**(1), 67–108. Available from: https://doi.org/10.1093/plcell/koac263

Wang, K., **Durrett, T.P.** & **Benning, C.** (2019) Functional diversity of glycerolipid acylhydrolases in plant metabolism and physiology. *Progress in Lipid Research*, **75**, 100987. Available from: https://doi.org/10.1016/j.plipres.2019.100987

Weyers, J.D.B. & **Johansen, L.G.** (1985) Accurate estimation of stomatal aperture from silicone rubber impressions. *The New Phytologist*, **101**(1), 109–115. Available from: https://doi.org/10.1111/j.1469-8137.1985.tb02820.x

Wickramanayake, J.S. & **Czymmek, K.J.** (2023) A conventional fixation volume electron microscopy protocol for plants. *Methods in Cell Biology*, **177**, 83–99. Available from: https://doi.org/10.1016/bs.mcb.2023.04.008

Yurchenko, O., **Kimberlin, A.**, **Mehling, M.**, **Koo, A.J.**, **Chapman, K.D.**, **Mullen, R.T.** ***et al.*** (2018) Response of high leaf-oil *Arabidopsis thaliana* plant lines to biotic or abiotic stress. *Plant Signaling & Behavior*, **13**(5), e1464361. Available from: https://doi.org/10.1080/15592324.2018.1464361

Zhu, T., **De Lima, C.F.F.** & **De Smet, I.** (2021) The heat is on: how crop growth, development and yield respond to high temperature. *Journal of Experimental Botany*, **72**(21), 7359–7373. Available from: https://doi.org/10.1093/jxb/erab308